

Graphical Abstract

Optimal convergence in finite element fully discrete error analysis and a novel fast solver for the Doyle-Fuller-Newman model of lithium-ion batteries *

Shu Xu, Liqun Cao

Highlights

Optimal convergence in finite element fully discrete error analysis and a novel fast solver for the Doyle-Fuller-Newman model of lithium-ion batteries

Shu Xu, Liqun Cao

- Comprehensive numerical analysis and implementation of the most widely used multiscale and multiphysics model for lithium-ion batteries.
- Optimal-order error estimates in the norms $l^2(H^1)$ and $l^2(L^2(H_r^q))$, $q = 0, 1$, are rigorously established.
- Numerical convergence rates in both 2D and 3D are validated, which is unaccessible in the literature.
- A novel solver is designed to accelerate computation, effectively handling strong nonlinearity and multiscale complexity.
- Three-dimensional numerical experiments with real battery parameters demonstrate that the proposed solver is faster than its rivals.

Optimal convergence in finite element fully discrete error analysis and a novel fast solver for the Doyle-Fuller-Newman model of lithium-ion batteries

Shu Xu^{a,b}, Liqun Cao^{b,c,d,*}

^a*School of Mathematical Sciences, Peking University, Beijing, 100871, China*

^b*Institute of Computational Mathematics and Scientific/Engineering Computing,
Academy of Mathematics and Systems Science, Chinese Academy of
Sciences, Beijing, 100190, China*

^c*State Key Laboratory of Scientific and Engineering Computing, Beijing, 100190, China*

^d*National Center for Mathematics and Interdisciplinary Sciences, Chinese Academy of
Sciences, Beijing, 100190, China*

Abstract

We investigate the convergence of a backward Euler finite element discretization applied to a multi-domain and multi-scale elliptic-parabolic system, derived from the Doyle-Fuller-Newman model for lithium-ion batteries. Our analysis establishes optimal-order error estimates for variables in the norms $l^2(H^1)$ and $l^2(L^2(H_r^q))$, $q = 0, 1$. To enhance computational efficiency, we introduce a novel scale-decoupled solver that balances rapid convergence with reduced memory requirements. Numerical experiments using realistic battery parameters validate the theoretical error rates and highlight the superior performance of the proposed solver compared to existing algorithms.

Keywords: Elliptic-parabolic system, Lithium-ion batteries, DFN model, Finite element, Error analysis, Multiscale and multiphysics model

2020 MSC: 65M15, 65M60, 65N15, 65N30, 78A57

*This work was funded by the National Natural Science Foundation of China (grant 12371437) and the Beijing Natural Science Foundation (grant Z240001).

*Corresponding author

Email addresses: xushu@lsec.cc.ac.cn (Shu Xu), c1q@lsec.cc.ac.cn (Liqun Cao)

1. Introduction

The Doyle-Fuller-Newman (DFN) model [1, 2], commonly referred to as the pseudo-two-dimensional (P2D) model when the battery region is simplified to one dimension, is the most widely used physics-based model for lithium-ion batteries. It is essential in various engineering applications, including estimating the state of charge (SOC), analyzing capacity performance under diverse operating conditions, and generating impedance spectra [3, 4, 5, 6, 7, 8]. Furthermore, as a cornerstone of battery modeling, it provides a robust foundation for incorporating additional physics, such as temperature effects and mechanical stress, enabling various model extensions [9, 10, 11, 12].

In this paper, we examine the following fully coupled nonlinear elliptic-parabolic system that characterizes the DFN model:

$$\begin{cases} -\nabla \cdot (\kappa_1 \nabla \phi_1 - \kappa_2 \nabla f(c_1)) = a_2 J, & (x, t) \in \Omega_1 \times (0, T), \\ -\nabla \cdot (\sigma \nabla \phi_2) = -a_2 J, & (x, t) \in \Omega_2 \times (0, T), \\ \varepsilon_1 \frac{\partial c_1}{\partial t} - \nabla \cdot (k_1 \nabla c_1) = a_1 J, & (x, t) \in \Omega_1 \times (0, T), \\ \frac{\partial c_2}{\partial t} - \frac{1}{r^2} \frac{\partial}{\partial r} (r^2 k_2 \frac{\partial c_2}{\partial r}) = 0, & (x, r, t) \in \Omega_{2r} \times (0, T), \end{cases} \quad (1)$$

where $\Omega_2 \subset \Omega_1 \subset \mathbb{R}^N$ and $\Omega_{2r} \subset \mathbb{R}^N \times \mathbb{R}_+$, $N = 1, 2, 3$, represent multiply connected domains. It is notable that the last equation does not involve x -differential operators, and Ω_{2r} spans two distinct scales x and r . Specifically, for each point $x \in \Omega_2$, there exists a singular parabolic equation defined over the r -coordinate.

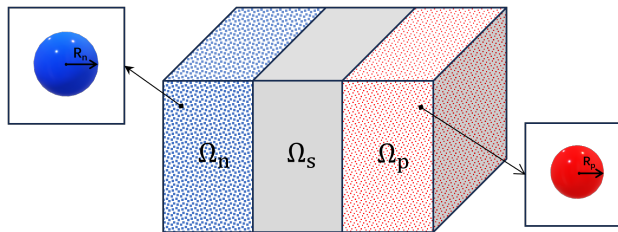


Figure 1: A 3D schematic representation of a Li-ion battery.

In the DFN model, a lithium-ion battery occupies a domain $\Omega \subset \mathbb{R}^N$, where $1 \leq N \leq 3$, comprising three subdomains: the positive electrode Ω_p , the negative electrode Ω_n , and the separator Ω_s . These regions form a laminated box structure, with $\bar{\Omega} = \bar{\Omega}_n \cup \bar{\Omega}_s \cup \bar{\Omega}_p$, as illustrated in Figure 1.

Following a macrohomogeneous approach, it is assumed that the electrode and electrolyte phases coexist within Ω_2 , and spherical particles with radii R_p and R_n are uniformly distributed throughout the electrodes, parameterized by the coordinates $(x, r) \in \Omega_{2r} := (\Omega_n \times (0, R_n)) \cup (\Omega_p \times (0, R_p))$. We define the electrolyte region as $\Omega_1 = \Omega_n \cup \Omega_s \cup \Omega_p$ and the electrode region as $\Omega_2 = \Omega_n \cup \Omega_p$. The model seeks to solve for four key variables: the electrolyte potential $\phi_1(x, t)$, the electrode potential $\phi_2(x, t)$, the lithium-ion concentration in the electrolyte $c_1(x, t)$, and the lithium concentration within the particles $c_2(x, r, t)$.

The multi-domain characteristics of the DFN model imply that the coefficients and nonlinear functions exhibit discontinuities across subdomains. Let $\mathbf{1}_{\Omega_m}$ denote the indicator function for the subdomain Ω_m . It is assumed that $\varepsilon_1, \sigma, k_i$ and a_i ($i = 1, 2$), are piecewisely positive constants. For the coefficients κ_i , $i = 1, 2$, we define

$$\kappa_i = \sum_{m \in \{n, s, p\}} \kappa_{im}(c_1) \mathbf{1}_{\Omega_m}, \quad (2)$$

where $\kappa_{1m}, \kappa_{2m}: (0, +\infty) \rightarrow (0, +\infty)$. For the spherical particles in the electrode regions, we set the radii as $R_s = \sum_{m \in \{n, p\}} R_m \mathbf{1}_{\Omega_m}$ and the maximum lithium concentration as $c_{2,\max} = \sum_{m \in \{n, p\}} c_{2,\max,m} \mathbf{1}_{\Omega_m}$. The source term J depends on the lithium concentration at the particle surface, $\bar{c}_2(x, t) = c_2(x, R_s(x), t)$, and $\eta := \phi_2 - \phi_1 - U$, where $U = \sum_{m \in \{n, p\}} U_m(\bar{c}_2) \mathbf{1}_{\Omega_m}$, and $U_m: (0, c_{2,\max,m}) \rightarrow \mathbb{R}$. Then, J is expressed as

$$J = \sum_{m \in \{n, p\}} J_m(c_1, \bar{c}_2, \eta) \mathbf{1}_{\Omega_m}, \quad (3)$$

where $J_m: (0, +\infty) \times (0, c_{2,\max,m}) \times \mathbb{R} \rightarrow \mathbb{R}$. In addition, we set $\underline{v} = \min_x v$ and $\bar{v} = \max_x v$, when v is piecewise constant. However, $f: (0, +\infty) \rightarrow \mathbb{R}$ is assumed to be independent of spatial coordinates.

To complete the system, we introduce the initial conditions,

$$\begin{aligned} c_1(x, 0) &= c_{10}(x) > 0, \quad x \in \Omega_1, \\ c_2(x, r, 0) &= c_{20}(x, r), \quad 0 < c_{20}(x, r) < c_{2,\max}(x), \quad (x, r) \in \Omega_{2r}, \end{aligned}$$

the boundary conditions with a given function $I: \Gamma \rightarrow \mathbb{R}$ and a constant F ,

$$\begin{aligned} & -(\kappa_1 \nabla \phi_1 - \kappa_2 \nabla f(c_1)) \cdot \mathbf{n}|_{\partial\Omega} = 0, \\ & -\sigma \nabla \phi_2 \cdot \mathbf{n}|_{\Gamma} = I, \quad -\sigma \nabla \phi_2 \cdot \mathbf{n}|_{\partial\Omega_2 \setminus \Gamma} = 0, \\ & -k_1 \nabla c_1 \cdot \mathbf{n}|_{\partial\Omega} = 0, \\ & -r^2 k_2 \frac{\partial c_2(x)}{\partial r} \Big|_{r=0} = 0, \quad -r^2 k_2 \frac{\partial c_2(x)}{\partial r} \Big|_{r=R_s(x)} = \frac{J(x)}{F}, \quad x \in \Omega_2, \end{aligned} \quad (4)$$

and the interface conditions

$$\begin{aligned} [\![\phi_1]\!]_{\Gamma_{sk}} &= 0, \quad [\![(\kappa_1 \nabla \phi_1 - \kappa_2 \nabla f(c_1)) \cdot \boldsymbol{\nu}]\!]_{\Gamma_{sk}} = 0, \quad k \in \{n, p\}, \\ [\![c_1]\!]_{\Gamma_{sk}} &= 0, \quad [\![k_1 \nabla c_1 \cdot \boldsymbol{\nu}]\!]_{\Gamma_{sk}} = 0, \quad k \in \{n, p\}, \end{aligned}$$

where \mathbf{n} denotes the outward unit normal vector, Γ is a measurable subset of $\partial\Omega_2$ with positive measure, Γ_{sn} and Γ_{sp} are the separator-negative and separator-positive interfaces respectively, $[\![v]\!]_{\Sigma}$ represents the jump of a quantity v across the interface Σ , and $\boldsymbol{\nu}$ denotes the outward unit normal vector at $\partial\Omega_s$.

Remark 1.1. Apart from making the coupling quasilinear by the coefficients (2), the coupling is influenced by the nonlinear function J on the right-hand side of (1) and the Neumann boundary condition (4), which represents the homogenization process and the electrochemical coupling between the electrode scale and the particle scale..

More specifically, the DFN model is a particular case of the more general mathematical formulation (1), when $\kappa_2 = \frac{2RT}{F}\kappa_1(1 - t_+^0)$, $f = \ln$, and J is governed by the Butler-Volmer equation [13]. For a detailed derivation of the DFN model, we recommend referring to [2, 14, 15, 16, 17]. As noted by [18], the change of variables for ϕ_1 is avoided, ensuring that the finite element error analysis in this original formulation is also applicable to non-uniform temperature distributions.

With function spaces and notations introduced in Appendix A, the weak solution of (1) can be defined as a quadruplet $(\phi_1, \phi_2, c_1, c_2)$,

$$\begin{aligned} \phi_1 &\in L^2(0, T; H_*^1(\Omega)), \quad \phi_2 \in L^2(0, T; H^1(\Omega_2)), \\ c_1 &\in C([0, T]; L^2(\Omega)) \cap L^2(0, T; H^1(\Omega)), \quad \frac{\partial c_1}{\partial t} \in L^2(0, T; L^2(\Omega)), \\ c_2 &\in C([0, T]; L^2(\Omega_2; L_r^2(0, R_s(\cdot)))) \cap L^2(0, T; L^2(\Omega_2; H_r^1(0, R_s(\cdot)))), \\ \frac{\partial c_2}{\partial t} &\in L^2(0, T; L^2(\Omega_2; L_r^2(0, R_s(\cdot)))) , \end{aligned}$$

such that $c_1(0) = c_{10}$, $c_2(0) = c_{20}$, and for $t \in (0, T)$ a.e.,

$$\int_{\Omega} \kappa_1(t) \nabla \phi_1(t) \cdot \nabla \varphi \, dx - \int_{\Omega} \kappa_2(t) \nabla f(c_1(t)) \cdot \nabla \varphi \, dx - \int_{\Omega_2} a_2 J(t) \varphi \, dx = 0, \\ \forall \varphi \in H_*^1(\Omega), \quad (5)$$

$$\int_{\Omega_2} \sigma \nabla \phi_2(t) \cdot \nabla \varphi \, dx + \int_{\Omega_2} a_2 J(t) \varphi \, dx + \int_{\Gamma} I(t) \varphi \, ds = 0, \quad \forall \varphi \in H^1(\Omega_2), \quad (6)$$

$$\int_{\Omega} \varepsilon_1 \frac{dc_1}{dt}(t) \varphi \, dx + \int_{\Omega} k_1 \nabla c_1(t) \cdot \nabla \varphi \, dx - \int_{\Omega_2} a_1 J(t) \varphi \, dx = 0, \quad \forall \varphi \in H^1(\Omega), \\ (7)$$

$$\int_{\Omega_2} \int_0^{R_s(x)} \frac{dc_2}{dt}(t) \psi r^2 \, dr \, dx + \int_{\Omega_2} \int_0^{R_s(x)} k_2 \frac{\partial c_2(t)}{\partial r} \frac{\partial \psi}{\partial r} r^2 \, dr \, dx + \\ \int_{\Omega_2} \frac{R_s^2(x)}{F} J(t, x) \psi(x, R_s(x)) \, dx = 0, \quad \forall \psi \in L^2(\Omega_2; H_r^1(0, R_s(\cdot))). \quad (8)$$

Under certain assumptions on the data, local existence and uniqueness of the solution to the DFN model for $\dim \Omega = 1$ was established by [19, 20]. Moreover, the solution can be extended to a globally unique solution under specific conditions [20]. However, the problem of existence and uniqueness remains open for the case of $\dim \Omega = 2, 3$. The main mathematical challenges in this context include the strongly nonlinear source terms with singular behaviour, discontinuous and nonlinear coefficients, the lack of smoothness of the boundary and the pseudo- $(N+1)$ -dimensional equation.

Efficient simulation of the DFN model continues to be an active area of research. Various spatial discretization methods have been employed to convert the system of PDEs to a system of DAEs. These include the finite element method [21, 13, 22, 16], finite difference method [2, 23, 24, 25], finite volume method [26, 27], collocation method [28, 29], and hybrid method [3, 30]. To achieve full discretization, computationally efficient time-stepping algorithms are applied, such as those detailed in [31, 13, 32, 33]. Among these methods, the finite element method is particularly advantageous for handling irregular geometries, unconventional boundary conditions, heterogeneous compositions, and ensuring global conservation. As a result, it is increasingly adopted in battery modeling software [32, 34, 35, 36]. Additionally,

the backward Euler method is commonly employed due to its unconditional stability [27, 34, 37, 38, 39].

Despite notable advancements in numerical methods for the DFN model, research on rigorous error analysis remains limited [22, 18]. The work in [22] was the first to present a convergence analysis of the backward Euler finite element discretization of this model. However, the analysis has limitations: it is inapplicable for the cases $N = 2, 3$, where the imbedding $H^1(D_2) \hookrightarrow C(\bar{D}_2)$ fails and it requires additional assumptions or efforts to validate the interpolation operator I_0^x used therein. Furthermore, the theoretical convergence rates presented do not align with observed numerical results. Recently, a novel approach to estimating the error for c_2 was proposed in [18]. This approach utilizes a multiscale or pseudo- $(N+1)$ -dimensional projection, which aligns the analysis with the established framework from [40]. Additionally, the inclusion of trace error estimation enabled proving optimal-order convergence concerning the radial mesh size. The primary aim of this paper is to extend the semi-discrete error analysis presented in [18] to the fully discrete setting, addressing the gaps associated with the backward Euler full discretization.

When the full discretization results in a large system of nonlinear algebraic equations, an efficient solver is urgently needed to enhance simulation efficiency for practical applications. Existing algorithms can be broadly categorized into fully coupled [23, 32, 41] and decoupling algorithms [9, 27, 42, 13, 39]. From the perspective of numerical algebra, both types correspond to block nonlinear Gauss-Seidel methods [43, 44], differing primarily in how the problem is partitioned into blocks. Fully coupled algorithms solve all unknown variables simultaneously using Newton's method. This approach often converges quickly due to the comprehensive coupling of all equations but can demand significant computational resources for storage and time due to the size of the blocks being solved. Decoupling algorithms handle the coupling between the governing PDEs by introducing an outer iteration loop. Each subproblem within this loop is solved separately, without requiring full accuracy, using an appropriate nonlinear solver in an inner iteration loop. This method reduces the per-block computational cost but may converge more slowly due to weaker coupling between blocks. In general, algorithms with larger blocks that couple more PDEs tend to converge faster but come at the cost of increased storage and computational burden for solving the subproblems. To optimize performance, a balance between convergence speed and computational efficiency must be achieved, motivating the development

of innovative solvers tailored to the specific requirements of the system.

The challenges in designing efficient solvers for the DFN model primarily stem from the strong nonlinear reaction term and its multiscale nature. The reaction term J , governed by the Butler-Volmer equation [45], involves complex mathematical functions like exponentials and power roots, which hinder convergence and reduce robustness in standard numerical solvers. To address these difficulties, fully coupled and tailored decoupling algorithms [32, 13, 39] have been developed, offering improved convergence and robustness properties. Additionally, the pseudo- $(N+1)$ -dimensional equation introduces an extra dimension, significantly increasing computational costs and memory demands. This motivates the development of scale-decoupled algorithms [9, 42, 13] which decouple the pseudo- $(N+1)$ -dimensional PDE. Furthermore, [46] emphasized the importance of understanding the physics of the problem and the effect of the extent of coupling on simulation times using a similar battery model. Building on these challenges and insights, this paper presents a novel scale-decoupled algorithm to accelerate computation while maintaining relatively low memory requirements.

The primary contributions of this paper are threefold. First, based on the finite element semi-discretization in [18], we propose the corresponding backward Euler finite element discretization and achieves error estimates with optimal convergence rates for $N = 1, 2, 3$. Second, we introduce a novel scale-decoupled algorithm that strategically addresses the system's strong nonlinearity. This significantly accelerates the convergence of the outer iteration while maintaining low memory overhead, making the algorithm particularly suitable for large-scale 2D/3D problems. Finally, we validate the numerical convergence rates in 2D and 3D using real battery parameters and provide a comprehensive comparison with existing scale-decoupled solvers. To the best of our knowledge, such numerical verification and comparison have not been previously reported in the literature.

The paper is structured as follows. Section 2 presents the backward Euler finite element discretization and derives error estimates with optimal convergence rates. Section 3 introduces a novel scale-decoupled solver to accelerate the solution. Section 4 reports numerical experiments using real battery parameters to validate our error estimates and evaluate the solver's performance. Finally, conclusions are drawn in section 5.

2. Error analysis of finite element fully-discrete problems

In this section, we only consider $\bar{\Omega}_m \subset \mathbb{R}^N$, $m \in \{n, s, p\}$ as polygonal domains such that $\bar{\Omega}_m$ is the union of a finite number of polyhedra. Let $\mathcal{T}_{h,m}$ be a regular family of triangulation for $\bar{\Omega}_m$, $m \in \{n, s, p\}$, and the meshes match at the interfaces, i.e., the points, edges and faces of discrete elements fully coincide at the interface. Hence, $\mathcal{T}_h := \bigcup_{m \in \{n, s, p\}} \mathcal{T}_{h,m}$ is also a regular family of triangulation for $\bar{\Omega}$. Additionally, it is assumed that all (K, P_K, Σ_K) , $K \in \mathcal{T}_h$, are finite element affine families [47]. For the closed interval $[0, R_s(x)]$, $x \in \Omega_2$, let $\mathcal{T}_{\Delta_r}(x)$ be a family of regular meshes, such that $[0, R_s(x)] = \bigcup_{I \in \mathcal{T}_{\Delta_r}(x)} I$. It is also assumed that each element of $\mathcal{T}_{\Delta_r}(x)$ is affine equivalent to a reference element. Since R_s is piecewise constant, here only two sets of meshes are considered, i.e.,

$$\mathcal{T}_{\Delta_r}(x) = \begin{cases} \mathcal{T}_{\Delta_r p}, & x \in \Omega_p, \\ \mathcal{T}_{\Delta_r n}, & x \in \Omega_n. \end{cases}$$

For each element $K \in \mathcal{T}_h$ and $I \in \bigcup_{x \in \Omega_2} \mathcal{T}_{\Delta_r}(x)$, we use h_K and Δr_I for the diameter respectively. Let $h = \max_{K \in \mathcal{T}_h} h_K$ and $\Delta r = \max_{I \in \bigcup_{x \in \Omega_2} \mathcal{T}_{\Delta_r}(x)} \Delta r_I$.

The unknowns ϕ_1 , ϕ_2 and c_1 are discretized by piecewise-linear elements. Let $V_h^{(1)}(\bar{\Omega})$ and $V_h^{(1)}(\bar{\Omega}_2)$ be the corresponding finite element spaces for c_1 and ϕ_2 , while

$$W_h(\bar{\Omega}) = \left\{ w_h \in V_h^{(1)}(\bar{\Omega}) : \int_{\Omega} w_h(x) dx = 0 \right\},$$

for ϕ_1 . For the pseudo- $(N+1)$ dimensional c_2 , piecewise-constant elements are used for discretization in the x coordinate while piecewise-linear elements in the r coordinate. Namely, a tensor product finite element space

$$V_{h\Delta r}(\bar{\Omega}_{2r}) := \left(V_h^{(0)}(\bar{\Omega}_n) \otimes V_{\Delta r}^{(1)}[0, R_n] \right) \bigcap \left(V_h^{(0)}(\bar{\Omega}_p) \otimes V_{\Delta r}^{(1)}[0, R_p] \right) \quad (9)$$

is used.

In order to obtain a full discretization, we consider a uniform mesh for the time variable t . Define $t_k := k\Delta t$, $k = 0, 1, \dots, K$, $\Delta t > 0$ being the time-step, and $K := [T/\Delta t]$, the integral part of $T/\Delta t$. By means of the backward Euler method, finite element fully discrete problems for (5)-(8) are proposed as follows:

Given $(c_{1h}^0, c_{2h\Delta r}^0) \in V_h^{(1)}(\bar{\Omega}) \times V_{h\Delta r}(\bar{\Omega}_{2r})$, $c_{1h}^0(x) > 0$, $0 < c_{2h\Delta r}^0(x, r) < c_{2,\max}(x)$, find $(\phi_{1h}^k, \phi_{2h}^k, c_{1h}^k, c_{2h\Delta r}^k) \in W_h(\bar{\Omega}) \times V_h^{(1)}(\bar{\Omega}_2) \times V_h^{(1)}(\bar{\Omega}) \times V_{h\Delta r}(\bar{\Omega}_{2r})$, $k = 1, \dots, K$, such that

$$\int_{\Omega} \kappa_{1h}^k \nabla \phi_{1h}^k \cdot \nabla w_h \, dx - \int_{\Omega} \kappa_{2h}^k \nabla f(c_{1h}^k) \cdot \nabla w_h \, dx - \int_{\Omega_2} a_2 J_h^k w_h \, dx = 0, \quad \forall w_h \in W_h(\bar{\Omega}), \quad (10)$$

$$\int_{\Omega_2} \sigma \nabla \phi_{2h}^k \cdot \nabla v_h \, dx + \int_{\Omega_2} a_2 J_h^k v_h \, dx + \int_{\Gamma} I^k v_h \, dx = 0, \quad \forall v_h \in V_h^{(1)}(\bar{\Omega}_2), \quad (11)$$

$$\int_{\Omega} \varepsilon_1 \frac{c_{1h}^k - c_{1h}^{k-1}}{\tau} v_h \, dx + \int_{\Omega} k_1 \nabla c_{1h}^k \cdot \nabla v_h \, dx - \int_{\Omega_2} a_1 J_h^k v_h \, dx = 0, \quad \forall v_h \in V_h^{(1)}(\bar{\Omega}) \quad (12)$$

$$\begin{aligned} & \int_{\Omega_2} \int_0^{R_s(x)} \frac{c_{2h\Delta r}^k - c_{2h\Delta r}^{k-1}}{\tau} v_{h\Delta r} r^2 \, dr \, dx + \int_{\Omega_2} \int_0^{R_s(x)} k_2 \frac{\partial c_{2h\Delta r}^k}{\partial r} \frac{\partial v_{h\Delta r}}{\partial r} r^2 \, dr \, dx \\ & + \int_{\Omega_2} \frac{R_s^2(x)}{F} J_h^k(x) v_{h\Delta r}(x, R_s(x)) \, dx = 0, \quad \forall v_{h\Delta r} \in V_{h\Delta r}(\bar{\Omega}_{2r}), \end{aligned} \quad (13)$$

where

$$\kappa_{ih}^k = \sum_{m \in \{n, s, p\}} \kappa_{im}(c_{1h}^k) \mathbf{1}_{\Omega_m}, \quad i = 1, 2, \quad J_h^k = \sum_{m \in \{n, p\}} J_m(c_{1h}^k, \bar{c}_{2h}^k, \eta_h^k) \mathbf{1}_{\Omega_m},$$

$$\bar{c}_{2h}^k(x) := c_{2h\Delta r}^k(x, R_s(x)), \quad \eta_h^k = \phi_{2h}^k - \phi_{1h}^k - U_h^k, \quad U_h^k = \sum_{m \in \{n, p\}} U_m(\bar{c}_{2h}^k) \mathbf{1}_{\Omega_m}.$$

To present the finite element error analysis, we need to make the following assumptions.

Hypothesis 2.1. $f \in C^1(0, +\infty)$. For $m \in \{n, p\}$, $\kappa_{1m}, \kappa_{2m} \in C^2(0, +\infty)$, $U_m \in C^2(0, c_{2,\max,m})$, $J_m \in C^1((0, +\infty) \times (0, c_{2,\max,m}) \times \mathbb{R})$ and

$$\exists \alpha > 0: \forall (c_1, \bar{c}_2, \eta) \in (0, +\infty) \times (0, c_{2,\max,m}) \times \mathbb{R}, \quad \frac{\partial J_m}{\partial \eta}(c_1, \bar{c}_2, \eta) \geq \alpha.$$

Hypothesis 2.2. $c_{10} \in H_{\text{pw}}^2(\Omega_1)$, $c_{20} \in H^1(\Omega_2; H_r^1(0, R_s(\cdot))) \cap L^2(\Omega_2; H_r^2(0, R_s(\cdot)))$. $c_{10}(x) > 0$, $x \in \Omega_2$ a.e., $0 < c_{20}(x, r) < c_{2,\max}(x)$, $(x, r) \in \Omega_{2r}$ a.e.. $I \in L^2(0, T; L^2(\Gamma))$.

Hypothesis 2.3.

$$\begin{aligned} \phi_1 &\in C\left([0, T]; H_{\text{pw}}^2(\Omega_1)\right), \phi_2 \in C\left([0, T]; H_{\text{pw}}^2(\Omega_2)\right), c_1 \in H^1\left(0, T; H_{\text{pw}}^2(\Omega_1)\right), \\ c_2 &\in H^1\left(0, T; H^1\left(\Omega_2; H_r^1(0, R_s(\cdot))\right) \cap L^2\left(\Omega_2; H_r^2(0, R_s(\cdot))\right)\right). \end{aligned}$$

Hypothesis 2.4. *There exist constants $L, M, N, Q > 0$ such that for $t \in [0, T]$ a.e.,*

$$\begin{aligned} \|\phi_i(t)\|_{L^\infty(\Omega_i)}, \|\phi_{ih}(t)\|_{L^\infty(\Omega_i)}, \|\nabla \phi_i(t)\|_{L^\infty(\Omega_i)}, \|\nabla \phi_{ih}(t)\|_{L^\infty(\Omega_i)} &\leq L, \quad i = 1, 2, \\ \frac{1}{M} \leq c_1(t), \quad c_{1h}(t) \leq M, \quad \frac{1}{N} \leq \frac{\bar{c}_2(t)}{c_{2,\max}}, \quad \frac{\bar{c}_{2h\Delta r}(t)}{c_{2,\max}} &\leq \left(1 - \frac{1}{N}\right), \\ \|\nabla c_1(t)\|_{L^\infty(\Omega)}, \|\nabla c_{1h}(t)\|_{L^\infty(\Omega)} &\leq Q. \end{aligned}$$

In addition, for a time-dependent variable $u(t)$, we use the notation $u^k = u(t_k)$ for brevity.

2.1. Auxiliary results

To analyze the finite element error for the multiscale system, it is essential to introduce several projection operators into finite element spaces, particularly tensor product spaces, along with their approximation properties.

Define the projection operator P_h from $H^1(\Omega)$ to $V_h^{(1)}(\bar{\Omega})$ such that $\forall u \in H^1(\Omega)$,

$$\int_{\Omega} k_1 \nabla(u - P_h u) \cdot \nabla \varphi_h \, dx + \int_{\Omega} (u - P_h u) \varphi_h \, dx = 0, \quad \forall \varphi_h \in V_h^{(1)}(\bar{\Omega}). \quad (14)$$

It is evident that P_h is well-defined, with the following approximation error [48]

$$\|u - P_h u\|_{H^1(\Omega)} \leq Ch \|u\|_{H_{\text{pw}}^2(\Omega_1)}. \quad (15)$$

Define the projection $P_{h\Delta r} : L^2(\Omega_2; H_r^1(0, R_s(\cdot))) \rightarrow V_{h\Delta r}(\bar{\Omega}_{2r})$,

$$\begin{aligned} \int_{\Omega_2} \int_0^{R_s(x)} \left(k_2 \frac{\partial(P_{h\Delta r} w - w)}{\partial r} \frac{\partial w_{h\Delta r}}{\partial r} + (P_{h\Delta r} w - w) w_{h\Delta r} \right) r^2 \, dr \, dx &= 0, \\ \forall w_{h\Delta r} \in V_{h\Delta r}(\bar{\Omega}_{2r}), \quad (16) \end{aligned}$$

and the projection error estimates [18] are given as follows:

Lemma 2.1. *If $w \in H^1(\Omega_2; H_r^1(0, R_s(\cdot))) \cap L^2(\Omega_2; H_r^2(0, R_s(\cdot)))$, then for $q = 0, 1$,*

$$\|w - P_{h\Delta r} w\|_{0,\Omega_2;q,r} \leq C(h\|w\|_{1,\Omega_2;1,r} + (\Delta r)^{2-q}\|w\|_{0,\Omega_2;2,r}).$$

Lemma 2.2. *If $w \in H^1(\Omega_2; H_r^1(0, R_s(\cdot))) \cap L^2(\Omega_2; H_r^2(0, R_s(\cdot)))$, we have*

$$\|(w - P_{h\Delta r} w)(\cdot, R_s(\cdot))\|_{0,\Omega_2} \leq C(h\|w\|_{1,\Omega_2;1,r} + (\Delta r)^2\|w\|_{0,\Omega_2;2,r}).$$

It can be seen from [18] that lemma 2.2 is crucial for establishing the optimal-order error estimates with respect to Δr .

2.2. Error estimation for c_1

By virtue of the projection operator P_h , the finite element error can be decomposed as follows:

$$c_1(t) - c_{1h}(t) = (c_1(t) - P_h c_1(t)) + (P_h c_1(t) - c_{1h}(t)) =: \rho_1(t) + \theta_1(t). \quad (17)$$

Since for $k = 0, 1$,

$$\|\rho_1(t)\|_{k,\Omega} \leq Ch\|c_1(t)\|_{2,\Omega_1} \leq Ch\left(\|c_{10}\|_{2,\Omega_1} + \int_0^t \left\| \frac{\partial c_1}{\partial t}(s) \right\|_{2,\Omega_1} ds\right), \quad (18)$$

it remains to estimate $\theta_1(t)$.

Next, since ε_1 is a piecewise positive constant function independent of time t , the norms $\left\| \varepsilon_1^{1/2} u \right\|_{L^2(\Omega)}$ and $\|u\|_{L^2(\Omega)}$ are equivalent. For simplicity, we assume $\varepsilon_1 \equiv 1$ in the subsequent analysis.

Lemma 2.3. *There exist an arbitrarily small number $\epsilon > 0$ and a positive constant C that do not depend on τ , h and Δr , such that for each $k = 1, \dots, K$,*

$$\begin{aligned} & \|\theta_1^k\|_{0,\Omega}^2 - \|\theta_1^{k-1}\|_{0,\Omega}^2 + \|\theta_1^k - \theta_1^{k-1}\|_{0,\Omega}^2 + 2\underline{k}_1\tau \|\nabla \theta_1^k\|_{0,\Omega}^2 \\ & \leq Ch^2 \left(\tau \|c_{10}\|_{2,\Omega_1}^2 + \tau \left\| \frac{\partial c_1}{\partial t} \right\|_{0;2,\Omega_1}^2 \right) + Ch^2 \left\| \frac{\partial c_1}{\partial t} \right\|_{0,k;2,\Omega_1}^2 + C\tau^2 \left\| \frac{\partial^2 c_1}{\partial t^2} \right\|_{0,k;0,\Omega}^2 \\ & \quad + C(\epsilon)\tau \|\theta_1^k\|_{0,\Omega}^2 + \epsilon\tau \left(\|\bar{c}_2^k - \bar{c}_{2h}^k\|_{0,\Omega_2}^2 + \|\phi_1^k - \phi_{1h}^k\|_{0,\Omega}^2 + \|\phi_2^k - \phi_{2h}^k\|_{0,\Omega_2}^2 \right). \end{aligned} \quad (19)$$

PROOF. The time derivative of c_1 at t_k is

$$\frac{\partial c_1}{\partial t}(t_k) = \frac{c_1(t_k) - c_1(t_{k-1})}{\tau} + \frac{1}{\tau} \int_{t_{k-1}}^{t_k} (s - t_{k-1}) \frac{\partial^2 c_1}{\partial t^2}(s) ds.$$

This leads to the decomposition of the temporal difference error as

$$\frac{\partial c_1}{\partial t}(t_k) - \frac{c_{1h}^k - c_{1h}^{k-1}}{\tau} = \frac{\rho_1^k - \rho_1^{k-1}}{\tau} + \frac{\theta_1^k - \theta_1^{k-1}}{\tau} + \int_{t_{k-1}}^{t_k} \left(\frac{s - t_{k-1}}{\tau} \right) \frac{\partial^2 c_1}{\partial t^2}(s) ds. \quad (20)$$

Hence taking $\varphi = v_h$ in (7) at $t = t_k$ and subtracting (12), it follows

$$\begin{aligned} & \int_{\Omega} (\theta_1^k - \theta_1^{k-1}) v_h dx + \tau \int_{\Omega} k_1 \nabla \theta_1^k \cdot \nabla v_h dx = \tau \int_{\Omega_2} a_1 (J^k - J_h^k) v_h dx dt \\ & - \int_{\Omega} (\rho_1^k - \rho_1^{k-1}) v_h dx - \int_{\Omega} \left(\int_{t_{k-1}}^{t_k} (s - t_{k-1}) \frac{\partial^2 c_1}{\partial t^2}(s) ds \right) v_h dx + \tau \int_{\Omega} \rho_1^k \cdot v_h dx. \end{aligned}$$

Next, by setting $v_h = \theta_1^k$, we have

$$\begin{aligned} & \frac{1}{2} \|\theta_1^k\|_{0,\Omega}^2 - \frac{1}{2} \|\theta_1^{k-1}\|_{0,\Omega}^2 + \frac{1}{2} \|\theta_1^k - \theta_1^{k-1}\|_{0,\Omega}^2 + k_1 \tau \|\nabla \theta_1^k\|_{0,\Omega}^2 \\ & \leq C \tau \|J^k - J_h^k\|_{0,\Omega_2} \|\theta_1^k\|_{0,\Omega} + C \|\rho_1^k - \rho_1^{k-1}\|_{0,\Omega} \|\theta_1^k\|_{0,\Omega} \\ & \quad + \tau^{\frac{3}{2}} \left\| \frac{\partial^2 c_1}{\partial t^2} \right\|_{0,k;0,\Omega} \|\theta_1^k\|_{0,\Omega} + \tau \|\rho_1^k\|_{0,\Omega} \|\theta_1^k\|_{0,\Omega}. \end{aligned} \quad (21)$$

Since Hypotheses 2.1 and 2.4 hold,

$$\begin{aligned} \|J^k - J_h^k\|_{0,\Omega_2} & \leq C \left(\|c_1^k - c_{1h}^k\|_{0,\Omega} + \|\bar{c}_2^k - \bar{c}_{2h}^k\|_{0,\Omega_2} + \|\phi_1^k - \phi_{1h}^k\|_{0,\Omega} + \|\phi_2^k - \phi_{2h}^k\|_{0,\Omega_2} \right) \\ & \leq C \left(\|\rho_1^k\|_{0,\Omega} + \|\theta_1^k\|_{0,\Omega} + \|\bar{c}_2^k - \bar{c}_{2h}^k\|_{0,\Omega_2} + \|\phi_1^k - \phi_{1h}^k\|_{0,\Omega} + \|\phi_2^k - \phi_{2h}^k\|_{0,\Omega_2} \right). \end{aligned} \quad (22)$$

We write

$$\rho_1^k - \rho_1^{k-1} = (I - P_h)(c_1^k - c_1^{k-1}) = (I - P_h) \int_{t_{k-1}}^{t_k} \frac{\partial c_1}{\partial t}(s) ds,$$

and obtain

$$\|\rho_1^k - \rho_1^{k-1}\|_{0,\Omega} \leq Ch \left\| \int_{t_{k-1}}^{t_k} \frac{\partial c_1}{\partial t}(s) ds \right\|_{2,\Omega_1} \leq Ch \tau^{\frac{1}{2}} \left\| \frac{\partial c_1}{\partial t} \right\|_{0,k;2,\Omega_1}.$$

By virtue of (18),

$$\|\rho_1^k\|_{0,\Omega} \leq Ch\|c_1(t_k)\|_{2,\Omega_1} \leq Ch \left(\|c_{10}\|_{2,\Omega_1} + \int_0^{t_k} \left\| \frac{\partial c_1}{\partial t}(s) \right\|_{2,\Omega_1} ds \right).$$

Together with the above estimates, Young's inequality implies that there exists $\epsilon > 0$, such that

$$\begin{aligned} & \|\theta_1^k\|_{0,\Omega}^2 - \|\theta_1^{k-1}\|_{0,\Omega}^2 + \|\theta_1^k - \theta_1^{k-1}\|_{0,\Omega}^2 + 2\underline{k}_1\tau \|\nabla \theta^k\|_{0,\Omega}^2 \\ & \leq Ch^2 \left(\tau \|c_{10}\|_{2,\Omega_1}^2 + \tau \left\| \frac{\partial c_1}{\partial t} \right\|_{0;2,\Omega_1}^2 \right) + Ch^2 \left\| \frac{\partial c_1}{\partial t} \right\|_{0,k;2,\Omega_1}^2 + C\tau^2 \left\| \frac{\partial^2 c_1}{\partial t^2} \right\|_{0,k;0,\Omega}^2 \\ & \quad + C(\epsilon)\tau \|\theta_1^k\|_{0,\Omega}^2 + \epsilon\tau \left(\|\bar{c}_2^k - \bar{c}_{2h}^k\|_{0,\Omega_2}^2 + \|\phi_1^k - \phi_{1h}^k\|_{0,\Omega}^2 + \|\phi_2^k - \phi_{2h}^k\|_{0,\Omega_2}^2 \right). \end{aligned}$$

2.3. Error estimation for c_2

Thanks to the projection operator $P_{h\Delta r}$, the finite element error for c_2 can be similarly decomposed as follows:

$$c_2(t) - c_{2h\Delta r}(t) = (c_2(t) - P_{h\Delta r}c_2(t)) + (P_{h\Delta r}c_2(t) - c_{2h\Delta r}(t)) =: \rho_2(t) + \theta_2(t), \quad (23)$$

and we have, setting $X = H^1(\Omega_2; H_r^1(0, R_s(\cdot))) \cap L^2(\Omega_2; H_r^2(0, R_s(\cdot)))$,

$$\begin{aligned} \|\rho_2(t)\|_{0,\Omega;q,r} & \leq Ch\|c_2(t)\|_{1,\Omega_2;1,r} + C(\Delta r)^{2-q}\|c_2(t)\|_{0,\Omega_2;q,r} \\ & \leq C(h + (\Delta r)^{2-q}) \left(\|c_{20}\|_X + \int_0^t \left\| \frac{\partial c_2}{\partial t}(s) \right\|_X ds \right), \quad q = 0, 1. \end{aligned} \quad (24)$$

We proceed to give an estimate for $\theta_2(t)$.

Lemma 2.4. *There exists an arbitrarily small number $\epsilon \in (0, 1)$ that does not depend on τ , h and Δr , such that for each $k = 1, \dots, K$,*

$$\begin{aligned} & \|\theta_2^k\|_{0,\Omega_2;0,r}^2 - \|\theta_2^{k-1}\|_{0,\Omega_2;0,r}^2 + \|\theta_2^k - \theta_2^{k-1}\|_{0,\Omega_2;0,r}^2 + 2\underline{k}_2\tau \left\| \frac{\partial \theta_2^k}{\partial r} \right\|_{0,\Omega_2;0,r}^2 \\ & \leq C(h^2 + (\Delta r)^4) \left(\tau \|c_{20}\|_X^2 + \tau \left\| \frac{\partial c_2}{\partial t} \right\|_{0;X}^2 + \left\| \frac{\partial c_2}{\partial t} \right\|_{0,k;X}^2 \right) + C\tau^2 \left\| \frac{\partial^2 c_2}{\partial t^2} \right\|_{0,k;0,\Omega_2;0,r}^2 \\ & \quad + C\epsilon\tau \left(\|c_1^k - c_{1h}^k\|_{0,\Omega}^2 + \|\phi_1^k - \phi_{1h}^k\|_{0,\Omega}^2 + \|\phi_2^k - \phi_{2h}^k\|_{0,\Omega_2}^2 \right) + C(\epsilon)\tau \|\theta_2^k\|_{0,\Omega_2;0,r}^2. \end{aligned} \quad (25)$$

PROOF. Similar to (20), the error of temporal difference can also be decomposed as

$$\frac{\partial c_2}{\partial t}(t_k) - \frac{c_{2h\Delta r}^k - c_{2h\Delta r}^{k-1}}{\tau} = \frac{\rho_2^k - \rho_2^{k-1}}{\tau} + \frac{\theta_2^k - \theta_2^{k-1}}{\tau} + \int_{t_{k-1}}^{t_k} \left(\frac{s - t_{k-1}}{\tau} \right) \frac{\partial^2 c_2}{\partial t^2}(s) ds.$$

Subtracting (13) from (8) at $t = t_k$, we obtain

$$\begin{aligned} & \int_{\Omega_2} \int_0^{R_s(x)} (\theta_2^k - \theta_2^{k-1}) v_{h\Delta r} r^2 dr dx + \tau \int_{\Omega_2} \int_0^{R_s(x)} k_2 \frac{\partial \theta_2^k}{\partial r} \frac{\partial v_{h\Delta r}}{\partial r} r^2 dr dx \\ &= - \int_{\Omega_2} \int_0^{R_s(x)} \left(\int_{t_{k-1}}^{t_k} (s - t_{k-1}) \frac{\partial^2 c_2}{\partial t^2}(s) ds \right) v_{h\Delta r} r^2 dr dx dt \\ & \quad - \int_{\Omega_2} \int_0^{R_s(x)} (\rho_2^k - \rho_2^{k-1}) v_{h\Delta r} r^2 dr dx + \tau \int_{\Omega_2} \int_0^{R_s(x)} \rho_2^k v_{h\Delta r} r^2 dr dx \\ & \quad - \tau \int_{\Omega_2} \frac{R_s^2}{F} (J^k - J_h^k) \bar{v}_h dx, \end{aligned} \tag{26}$$

where $\bar{v}_h := v_{h\Delta r}(x, R_s(x))$ and the penultimate term is due to (16).

We write

$$\rho_2^k - \rho_2^{k-1} = (I - P_{h\Delta r})(c_2^k - c_2^{k-1}) = (I - P_{h\Delta r}) \int_{t_{k-1}}^{t_k} \frac{\partial c_2}{\partial t}(s) ds,$$

and obtain

$$\|\rho_2^k - \rho_2^{k-1}\|_{0,\Omega_2;0,r} \leq C(h + (\Delta r)^2) \tau^{\frac{1}{2}} \left\| \frac{\partial c_2}{\partial t} \right\|_{0,k;X}.$$

For the last term, since $\|\bar{c}_2^k - \bar{c}_{2h}^k\|_{0,\Omega_2} \leq \|\bar{\rho}_2^k\|_{0,\Omega_2} + \|\bar{\theta}_2^k\|_{0,\Omega_2}$, it follows from (22) that

$$\begin{aligned} \|J^k - J_h^k\|_{0,\Omega_2} &\leq C \left(\|c_1^k - c_{1h}^k\|_{0,\Omega} + \|\bar{\rho}_2^k\|_{0,\Omega_2} + \|\bar{\theta}_2^k\|_{0,\Omega_2} \right. \\ &\quad \left. + \|\phi_1^k - \phi_{1h}^k\|_{0,\Omega} + \|\phi_2^k - \phi_{2h}^k\|_{0,\Omega_2} \right). \end{aligned} \tag{27}$$

By virtue of Lemma 2.2,

$$\begin{aligned} \|\bar{\rho}_2^k\|_{0,\Omega_2} &\leq Ch \|c_2(t_k)\|_{1,\Omega_2;1,r} + C(\Delta r)^2 \|c_2(t_k)\|_{0,\Omega_2;2,r} \\ &\leq C(h + (\Delta r)^2) \left(\|c_{20}\|_X + \int_0^{t_k} \left\| \frac{\partial c_2}{\partial t}(s) \right\|_X ds \right), \end{aligned} \tag{28}$$

and due to Proposition Appendix A.1, there is some $\epsilon_1 > 0$ to be determined later,

$$\|\bar{\theta}_2^k\|_{0,\Omega_2}^2 \leq \epsilon_1 \left\| \frac{\partial \theta_2^k}{\partial r} \right\|_{0,\Omega_2;0,r}^2 + C(\epsilon_1) \|\theta_2^k\|_{0,\Omega_2;0,r}^2. \quad (29)$$

Hence, Young's inequality yields for any $\epsilon_2 \in (0, 1)$,

$$\begin{aligned} & \int_{t_{k-1}}^{t_k} \int_{\Omega_2} \frac{R_s^2}{F} (J^k - J_h^k) \bar{v}_h \, dx ds \leq \epsilon_2 \tau \|J^k - J_h^k\|_{0,\Omega_2}^2 + C(\epsilon_2) \tau \|\bar{v}_h\|_{0,\Omega_2}^2 \\ & \leq C \tau (h^2 + (\Delta r)^4) \left(\|c_{20}\|_X^2 + \left\| \frac{\partial c_2}{\partial t} \right\|_{0;X}^2 \right) + C \epsilon_1 \tau \left\| \frac{\partial \theta_2^k}{\partial r} \right\|_{0,\Omega_2;0,r}^2 \\ & \quad + C \epsilon_2 \tau \left(\|c_1^k - c_{1h}^k\|_{0,\Omega}^2 + \|\phi_1^k - \phi_{1h}^k\|_{0,\Omega}^2 + \|\phi_2^k - \phi_{2h}^k\|_{0,\Omega_2}^2 \right) \\ & \quad + C(\epsilon_1) \tau \|\theta_2^k\|_{0,\Omega_2;0,r}^2 + C(\epsilon_2) \tau \|\bar{v}_h\|_{0,\Omega_2}^2. \end{aligned} \quad (30)$$

Finally, choosing $v_{h\Delta r} = \theta_2^k \in V_{h\Delta r}(\bar{\Omega}_{2r})$ in (26), and applying the Cauchy-Schwarz inequality along with (24), (29) and (30), we have

$$\begin{aligned} & \|\theta_2^k\|_{0,\Omega_2;0,r}^2 - \|\theta_2^{k-1}\|_{0,\Omega_2;0,r}^2 + \|\theta_2^k - \theta_2^{k-1}\|_{0,\Omega_2;0,r}^2 + 2\underline{k}_2 \tau \left\| \frac{\partial \theta_2^k}{\partial r} \right\|_{0,\Omega_2;0,r}^2 \\ & \leq C(h^2 + (\Delta r)^4) \left\| \frac{\partial c_2}{\partial t} \right\|_{0,k;X}^2 + C \tau (h^2 + (\Delta r)^4) \left(\|c_{20}\|_X^2 + \left\| \frac{\partial c_2}{\partial t} \right\|_{0;X}^2 \right) \\ & \quad + C \epsilon_2 \tau \left(\|c_1^k - c_{1h}^k\|_{0,\Omega}^2 + \|\phi_1^k - \phi_{1h}^k\|_{0,\Omega}^2 + \|\phi_2^k - \phi_{2h}^k\|_{0,\Omega_2}^2 \right) \\ & \quad + C(\epsilon_1, \epsilon_2) \tau \|\theta_2^k\|_{0,\Omega_2;0,r}^2 + C(\epsilon_2) \epsilon_1 \tau \left\| \frac{\partial \theta_2^k}{\partial r} \right\|_{0,\Omega_2;0,r}^2 + C \tau^2 \left\| \frac{\partial^2 c_2}{\partial t^2} \right\|_{0,k;0,\Omega_2;0,r}^2. \end{aligned}$$

Estimation (25) follows by choosing ϵ_1 sufficiently small.

2.4. Error estimation for the fully discrete problems

To this end, we still require error estimation for ϕ_1 and ϕ_2 , which will then be integrated with the previously derived results to address the fully coupled problem. The error estimations for ϕ_1 and ϕ_2 have already been provided in [18], and we restate the results here for completeness:

Proposition 2.1. *There is a constant C that does not depend on τ , h and Δr , such that*

$$\begin{aligned} & \|\phi_1(t_k) - \phi_{1h}^k\|_{1,\Omega}^2 + \|\phi_2(t_k) - \phi_{2h}^k\|_{1,\Omega_2}^2 \\ & \leq Ch^2 \left(\|\phi_1(t_k)\|_{2,\Omega_1}^2 + \|\phi_2(t_k)\|_{2,\Omega_2}^2 \right) \\ & \quad + C \left(\|c_1(t_k) - c_{1h}^k\|_{1,\Omega}^2 + \|\bar{c}_2(t_k) - \bar{c}_{2h}^k\|_{0,\Omega_2}^2 \right). \end{aligned}$$

Now, we are ready to establish the convergence result of this paper.

Theorem 2.1. *If Hypotheses 2.1-2.4 hold, there exists a constant C that does not depend on τ , h and Δr such that*

$$\begin{aligned} & \sum_{k=1}^K \tau \left(\|\phi_1^k - \phi_{1h}^k\|_{1,\Omega}^2 + \|\phi_2^k - \phi_{2h}^k\|_{1,\Omega_2}^2 + \|c_1^k - c_{1h}^k\|_{1,\Omega}^2 + \|\bar{c}_2^k - \bar{c}_{2h}^k\|_{0,\Omega_2}^2 \right) \\ & \leq C(h^2 + \tau^2 + (\Delta r)^4) + C \left(\|c_{10} - c_{10,h}\|_{0,\Omega}^2 + \|c_{20} - c_{20,h\Delta r}\|_{0,\Omega_2;0,r}^2 \right) \end{aligned} \tag{31}$$

$$\begin{aligned} & \sum_{k=1}^K \tau \|c_2^k - c_{2h\Delta r}^k\|_{0,\Omega_2;q,r}^2 \leq C(h^2 + \tau^2 + (\Delta r)^{4-2q}) \\ & \quad + C \left(\|c_{10} - c_{10,h}\|_{0,\Omega}^2 + \|c_{20} - c_{20,h\Delta r}\|_{0,\Omega_2;0,r}^2 \right), \quad q = 0, 1. \end{aligned} \tag{32}$$

PROOF. Combining Lemma 2.3 with Proposition 2.1, and utilizing (17), (18), (28) and (29), there is a constant ϵ_1 to be determined later, such that

$$\begin{aligned} & \|\theta_1^k\|_{0,\Omega}^2 - \|\theta_1^{k-1}\|_{0,\Omega}^2 + \|\theta_1^k - \theta_1^{k-1}\|_{0,\Omega}^2 + 2\underline{k}_1 \tau \|\nabla \theta^k\|_{0,\Omega}^2 \\ & \leq C(\epsilon_1) \tau \left(\|\theta_1^k\|_{0,\Omega}^2 + \|\theta_2^k\|_{0,\Omega_2;0,r}^2 \right) + C\epsilon_1 \tau \left(\|\nabla \theta_1^k\|_{0,\Omega}^2 + \left\| \frac{\partial \theta_2^k}{\partial r} \right\|_{0,\Omega_2;0,r}^2 \right) \\ & \quad + Ch^2 \left(\tau \|\phi_1^k\|_{2,\Omega_1}^2 + \tau \|\phi_2^k\|_{2,\Omega_2}^2 + \tau \|c_{10}\|_{2,\Omega_1}^2 + \tau \left\| \frac{\partial c_1}{\partial t} \right\|_{0;2,\Omega_1}^2 + \left\| \frac{\partial c_1}{\partial t} \right\|_{0,k;2,\Omega_1}^2 \right) \\ & \quad + C\tau^2 \left\| \frac{\partial^2 c_1}{\partial t^2} \right\|_{0,k;0,\Omega}^2 + C\tau(h^2 + (\Delta r)^4) \left(\|c_{20}\|_X^2 + \left\| \frac{\partial c_2}{\partial t} \right\|_{0;X}^2 \right). \end{aligned} \tag{33}$$

Again, combining Lemma 2.4 with Proposition 2.1, together with (17), (18), (28) and (29), there is also a constant $\epsilon_2 \in (0, 1)$ to be determined later, such that

$$\begin{aligned}
& \|\theta_2^k\|_{0,\Omega_2;0,r}^2 - \|\theta_2^{k-1}\|_{0,\Omega_2;0,r}^2 + \|\theta_2^k - \theta_2^{k-1}\|_{0,\Omega_2;0,r}^2 + 2\underline{k}_2\tau \left\| \frac{\partial \theta_2^k}{\partial r} \right\|_{0,\Omega_2;0,r}^2 \\
& \leq C(\epsilon_2) \tau \left(\|\theta_1^k\|_{0,\Omega}^2 + \|\theta_2^k\|_{0,\Omega_2;0,r}^2 \right) + C\epsilon_2\tau \left(\|\nabla \theta_1^k\|_{0,\Omega}^2 + \left\| \frac{\partial \theta_2^k}{\partial r} \right\|_{0,\Omega_2;0,r}^2 \right) \\
& \quad + C\tau h^2 \left(\|\phi_1^k\|_{2,\Omega_1}^2 + \|\phi_2^k\|_{2,\Omega_2}^2 + \|c_{10}\|_{2,\Omega_1}^2 + \left\| \frac{\partial c_1}{\partial t} \right\|_{0;2,\Omega_1}^2 \right) \\
& \quad + C(h^2 + (\Delta r)^4) \left(\tau \|c_{20}\|_X^2 + \tau \left\| \frac{\partial c_2}{\partial t} \right\|_{0;X}^2 + \left\| \frac{\partial c_2}{\partial t} \right\|_{0,k;X}^2 \right) \\
& \quad + C\tau^2 \left\| \frac{\partial^2 c_2}{\partial t^2} \right\|_{0,k;0,\Omega_2;0,r}^2. \tag{34}
\end{aligned}$$

Next, adding (33) and (34), and selecting ϵ_1, ϵ_2 sufficiently small, we have

$$\begin{aligned}
& \|\theta_1^k\|_{0,\Omega}^2 + \|\theta_2^k\|_{0,\Omega_2;0,r}^2 + \underline{k}_1\tau \|\nabla \theta_1^k\|_{0,\Omega}^2 + \underline{k}_2\tau \left\| \frac{\partial \theta_2^k}{\partial r} \right\|_{0,\Omega_2;0,r}^2 \\
& \leq \|\theta_1^{k-1}\|_{0,\Omega}^2 + \|\theta_2^{k-1}\|_{0,\Omega_2;0,r}^2 + C\tau \left(\|\theta_1^k\|_{0,\Omega}^2 + \|\theta_2^k\|_{0,\Omega_2;0,r}^2 \right) \\
& \quad + C\tau^2 \left(\left\| \frac{\partial^2 c_1}{\partial t^2} \right\|_{0,k;0,\Omega}^2 + \left\| \frac{\partial^2 c_2}{\partial t^2} \right\|_{0,k;0,\Omega_2;0,r}^2 \right) \\
& \quad + C\tau h^2 \left(\|\phi_1\|_{\infty;2,\Omega_1}^2 + \|\phi_2\|_{\infty;2,\Omega_2}^2 + \|c_{10}\|_{2,\Omega_1}^2 + \|c_{20}\|_X^2 \right) \\
& \quad + C\tau h^2 \left(\left\| \frac{\partial c_1}{\partial t} \right\|_{0;2,\Omega_1}^2 + \left\| \frac{\partial c_2}{\partial t} \right\|_{0;X}^2 \right) + C\tau(\Delta r)^4 \left(\|c_{20}\|_X^2 + \left\| \frac{\partial c_2}{\partial t} \right\|_{0;X}^2 \right) \\
& \quad + Ch^2 \left\| \frac{\partial c_1}{\partial t} \right\|_{0,k;2,\Omega_1}^2 + C(h^2 + (\Delta r)^4) \left\| \frac{\partial c_2}{\partial t} \right\|_{0,k;X}^2.
\end{aligned}$$

Discrete Gronwall's inequality yields

$$\begin{aligned}
& \|\theta_1^k\|_{0,\Omega}^2 + \|\theta_2^k\|_{0,\Omega_2;0,r}^2 + \sum_{l=1}^k \underline{k}_1 \tau \|\nabla \theta_1^l\|_{0,\Omega}^2 + \sum_{l=1}^k \underline{k}_2 \tau \left\| \frac{\partial \theta_2^l}{\partial r} \right\|_{0,\Omega_2;0,r}^2 \\
& \leq C \left(\|\theta_1^0\|_{0,\Omega}^2 + \|\theta_2^0\|_{0,\Omega_2;0,r}^2 \right) + C(\Delta r)^4 \left(\|c_{20}\|_X^2 + \left\| \frac{\partial c_2}{\partial t} \right\|_{0,X}^2 \right) \\
& \quad + Ch^2 \left(\|\phi_1\|_{\infty;2,\Omega_1}^2 + \|\phi_2\|_{\infty;2,\Omega_2}^2 + \|c_{10}\|_{2,\Omega_1}^2 + \|c_{20}\|_X^2 \right) \\
& \quad + Ch^2 \left(\left\| \frac{\partial c_1}{\partial t} \right\|_{0;2,\Omega_1}^2 + \left\| \frac{\partial c_2}{\partial t} \right\|_{0;X}^2 \right) + C\tau^2 \left(\left\| \frac{\partial^2 c_1}{\partial t^2} \right\|_{0;0,\Omega}^2 + \left\| \frac{\partial^2 c_2}{\partial t^2} \right\|_{0;0,\Omega_2;0,r}^2 \right) \\
& \leq C \left(\|\theta_1^0\|_{0,\Omega}^2 + \|\theta_2^0\|_{0,\Omega_2;0,r}^2 \right) + C (\tau^2 + h^2 + (\Delta r)^4).
\end{aligned}$$

Thus, we have the following $l^2(H^1)$ -norm estimation for c_1 , demonstrating the optimal order of convergence,

$$\begin{aligned}
\sum_{l=1}^k \tau \|c_1^l - c_{1h}^l\|_{1,\Omega}^2 & \leq \sum_{l=1}^k 2\tau \left(\|\rho_1^l\|_{1,\Omega}^2 + \|\theta_1^l\|_{0,\Omega}^2 + \|\nabla \theta_1^l\|_{0,\Omega}^2 \right) \\
& \leq Ch^2 + C\tau \sum_{l=1}^k \left(\|\theta_1^l\|_{0,\Omega}^2 + \|\nabla \theta_1^l\|_{0,\Omega}^2 \right) \\
& \leq C (\tau^2 + h^2 + (\Delta r)^4) + C \left(\|\theta_1^0\|_{0,\Omega}^2 + \|\theta_2^0\|_{0,\Omega_2;0,r}^2 \right),
\end{aligned}$$

and $l^2(L^2(H_r^q))$ -norm, $q = 0, 1$, for c_2

$$\begin{aligned}
\sum_{l=1}^k \tau \|c_2^l - c_{2h}^l\|_{0,\Omega_2;q,r}^2 & \leq \sum_{l=1}^k 2\tau \left(\|\rho_2^l\|_{0,\Omega_2;q,r}^2 + \|\theta_2^l\|_{0,\Omega_2;q,r}^2 \right) \\
& \leq C (\tau^2 + h^2 + (\Delta r)^{4-2q}) + C \left(\|\theta_1^0\|_{0,\Omega}^2 + \|\theta_2^0\|_{0,\Omega_2;0,r}^2 \right).
\end{aligned}$$

Further with $l^2(L^2)$ -norm estimation for \bar{c}_2 ,

$$\begin{aligned}
\sum_{l=1}^k \tau \|\bar{c}_2^l - \bar{c}_{2h}^l\|_{0,\Omega_2}^2 & \leq \sum_{l=1}^k C\tau \left(\|\bar{\rho}_2^l\|_{0,\Omega_2}^2 + \|\theta_2^l\|_{0,\Omega_2;0,r}^2 + \left\| \frac{\partial \theta_2^l}{\partial r} \right\|_{0,\Omega_2;0,r}^2 \right) \\
& \leq C (\tau^2 + h^2 + (\Delta r)^4) + C \left(\|\theta_1^0\|_{0,\Omega}^2 + \|\theta_2^0\|_{0,\Omega_2;0,r}^2 \right),
\end{aligned}$$

we also have $l^2(H^1)$ -norm estimation for ϕ_1 and ϕ_2 with the optimal order of convergence,

$$\begin{aligned} & \sum_{t=1}^k \tau \|\phi_1^t - \phi_1^t\|_{1,\Omega}^2 + \tau \|\phi_2^t - \phi_2^t\|_{1,\Omega_2}^2 \\ & \leq Ch^2 \left(\|\phi_1\|_{\infty;2,\Omega_1}^2 + \|\phi_2\|_{\infty;2,\Omega_2}^2 \right) + C \sum_{l=1}^k \left(\tau \|c_1^l - c_{1h}^l\|_{1,\Omega}^2 + \tau \|\bar{c}_2^l - \bar{c}_{2h}^l\|_{0,\Omega_2}^2 \right) \\ & \leq C (\tau^2 + h^2 + (\Delta r)^4) + C \left(\|\theta_1^0\|_{0,\Omega}^2 + \|\theta_2^0\|_{0,\Omega_2;0,r}^2 \right). \end{aligned}$$

Finally, notice that triangle inequality yields

$$\begin{aligned} \|\theta_1^0\|_{L^2(\Omega)} & \leq \|c_{10} - c_{1h}^0\|_{L^2(\Omega)} + Ch, \\ \|\theta_2^0\|_{L^2(\Omega_2;L_r^2(0,R_s(\cdot)))} & \leq \|c_{20} - c_{2h\Delta r}^0\|_{L^2(\Omega_2;L_r^2(0,R_s(\cdot)))} + C(h + (\Delta r)^2), \end{aligned}$$

which completes the proof.

3. A novel solver for the fully-discrete problems

In this section, we focus on efficiently solving the fully discrete system (10)-(13). We propose a novel fast solver, whose efficiency is demonstrated in subsection 4.2.

In the isothermal DFN model, the source term (3) is governed by the Butler-Volmer equation, which takes the following form:

$$J_m = k_m c_1^{\alpha_{a,m}} (c_{2,\max} - \bar{c}_2)^{\alpha_{a,m}} \bar{c}_2^{\alpha_{c,m}} \left(\exp \left(\frac{\alpha_{a,m} F}{RT_0} \eta_m \right) - \exp \left(\frac{-\alpha_{c,m} F}{RT_0} \eta_m \right) \right), \quad (35)$$

where $k_m, \alpha_{a,m} \in (0, 1)$, $\alpha_{c,m} \in (0, 1)$, F, R, T_0 are positive constants and

$$\eta_m = \phi_2 - \phi_1 - U_m(\bar{c}_2). \quad (36)$$

As seen in the equations of (1), the system is coupled through J , where the overpotential η appears in the exponential terms. Small variations in ϕ_1 , ϕ_2 and \bar{c}_2 , and consequently in η , can lead to large changes in J . This interdependency suggests that the solution can experience significant changes during each iteration, making the numerical solution process challenging. In fact, numerical experiments have confirmed that this behavior is indeed observed, supporting our conjecture.

Suppose that $\{\chi_i \psi_j\}_{i=1,\dots,M_2}^{j=1,\dots,N_i}$ is a set of basis functions for $V_{h\Delta r}(\bar{\Omega}_{2r})$, where $\chi_i = \mathbf{1}_{\hat{e}_i}$ and $\{\psi_j\}_{j=1,\dots,N_i}$ is the nodal basis for $V_{\Delta r}^{(1)}[0, R_m]$, for each $\hat{e}_i \in \mathcal{T}_{h,m}$, $m \in \{\text{n, p}\}$. Then for $c_{2h\Delta r}^k \in V_{h\Delta r}(\bar{\Omega}_{2r})$, the solution of the fully discrete problem at time step k is given by

$$c_{2h\Delta r}^k(x, r) = \sum_{i=1}^{M_2} \sum_{j=1}^{N_i} c_{2h\Delta r, ij}^k \chi_i(x) \psi_j(r).$$

Now, taking $v_{h\Delta r}(x, r) = \chi_i(x) \psi_{N_i}(r)$, $i = 1, \dots, M_2$ as the trial functions in (13), it follows that for $\hat{e}_i \in \mathcal{T}_{h,\text{n}} \cup \mathcal{T}_{h,\text{p}}$,

$$\begin{aligned} & \int_0^{R_m} \frac{c_{2h\Delta r, ij}^k - c_{2h\Delta r, ij}^{k-1}}{\tau} \psi_j \psi_{N_i} r^2 dr + \int_0^{R_m} k_2 c_{2h\Delta r, ij}^k \frac{\partial \psi_j}{\partial r} \frac{\partial \psi_{N_i}}{\partial r} r^2 dr \\ & + \frac{1}{|\hat{e}_i|} \int_{\hat{e}_i} \left(\frac{R_m^2}{F} J_m(c_{1h}^k, c_{2h\Delta r, iN_i}^k, \phi_{2h}^k - \phi_{1h}^k - U_m(c_{2h\Delta r, iN_i}^k)) \right) dx = 0. \end{aligned}$$

Note that the Einstein summation convention is used for the index j . If the macroscale variables c_{1h}^k , ϕ_{1h}^k and ϕ_{2h}^k are given, we can observe that only the above M_2 x -independent 1D equations need to solve for the microscopic c_2^k , which is suitable for parallel computing and avoids the significant memory overhead associated with computing the Jacobian.

These insights inspire us to design a scale-decoupled solver that solves ϕ_1 , ϕ_2 and \bar{c}_2 simultaneously, and then couples this with the rest in a sequential iteration procedure to accelerate convergence while maintaining low memory requirements.

Define $c_{2h\Delta r}^{k,n} \in V_{h\Delta r}(\bar{\Omega}_{2r})$ as the solution at iteration step n of the fully discrete problem at time step k , and we have

$$c_{2h\Delta r}^{k,n}(x, r) = \sum_{i=1}^{M_2} \sum_{j=1}^{N_i} c_{2h\Delta r, ij}^{k,n} \chi_i(x) \psi_j(r). \quad (37)$$

Additionally, introduce a temporary variable $c_{3h\Delta r}^{k,n+1} \in V_{h\Delta r}(\bar{\Omega}_{2r})$,

$$c_{3h\Delta r}^{k,n+1}(x, r) := \sum_{i=1}^{M_2} \sum_{j=1}^{N_i-1} c_{2h\Delta r, ij}^{k,n} \chi_i(x) \psi_j(r) + \sum_{i=1}^{M_2} c_{3h\Delta r, iN_i}^{k,n+1} \chi_i(x) \psi_{N_i}(r). \quad (38)$$

It can be observed that, once $c_{2h\Delta r}^{k,n}$ is known, the determination of $c_{3h\Delta r}^{k,n+1}$ only requires

$$\bar{c}_{3h}^{k,n+1}(x) := c_{3h\Delta r}^{k,n+1}(x, R_s(x)) = \sum_{i=1}^{M_2} c_{3h\Delta r, i N_i}^{k,n+1} \chi_i(x). \quad (39)$$

Let $(\phi_{1h}^{k-1}, \phi_{2h}^{k-1}, c_{1h}^{k-1}, c_{2h\Delta r}^{k-1})$ be the fully discrete solution at the $(k-1)$ th time step. To solve for the solution of the k -th time step, $(\phi_{1h}^k, \phi_{2h}^k, c_{1h}^k, c_{2h\Delta r}^k)$, we consider the following algorithm:

Step 0 (Initialization). Set initial values of iteration, $\phi_{1h}^{k,0} = \phi_{1h}^{k-1}$, $\phi_{2h}^{k,0} = \phi_{2h}^{k-1}$, $c_{1h}^{k,0} = c_{1h}^{k-1}$, $c_{2h\Delta r}^{k,0} = c_{2h\Delta r}^{k-1}$, $\bar{c}_{2h}^{k,0} = c_{2h\Delta r}^{k-1}(\cdot, R_s(\cdot))$, $U_h^{k,0} = \sum_{m \in \{\text{n,p}\}} U_m(\bar{c}_{2h}^{k,0}) \mathbf{1}_{\Omega_m}$, $\eta_h^{k,0} = \phi_{2h}^{k,0} - \phi_{1h}^{k,0} - U_h^{k,0}$, the relative iteration tolerance $rtol$ and the iteration step $n = 1$.

Step 1 (Subproblem (c_1)): Find $c_{1h}^{k,n} \in V_h^{(1)}(\bar{\Omega})$, such that for all $v_h \in V_h^{(1)}(\bar{\Omega})$,

$$\begin{aligned} & \int_{\Omega} \varepsilon_1 \frac{c_{1h}^{k,n} - c_{1h}^{k-1}}{\tau} v_h \, dx + \int_{\Omega} k_1 \nabla c_{1h}^{k,n} \cdot \nabla v_h \, dx \\ & - \int_{\Omega_2} \left(\sum_{m \in \{\text{n,p}\}} a_1 J_m(c_{1h}^{k,n}, \bar{c}_{2h}^{k,n-1}, \eta_h^{k,n-1}) \mathbf{1}_{\Omega_m} \right) v_h \, dx = 0. \end{aligned} \quad (40)$$

Step 2 (Subproblem $(\phi_1, \phi_2, \bar{c}_2)$): Find $\phi_{1h}^{k,n} \in W_h(\bar{\Omega})$, $\phi_{2h}^{k,n} \in V_h^{(1)}(\bar{\Omega}_2)$ and $c_{3h\Delta r}^{k,n} \in V_{h\Delta r}(\bar{\Omega}_{2r})$, such that for all $w_h \in W_h(\bar{\Omega})$, $v_h \in V_h^{(1)}(\bar{\Omega}_2)$, $v_{h\Delta r} \in V_{h\Delta r}(\bar{\Omega}_{2r})$,

$$\begin{aligned} & \int_{\Omega} \kappa_{1h}^{k,n} \nabla \phi_{1h}^k \cdot \nabla w_h \, dx - \int_{\Omega} \kappa_{2h}^{k,n} \nabla f(c_{1h}^{k,n}) \cdot \nabla w_h \, dx \\ & - \int_{\Omega_2} \left(\sum_{m \in \{\text{n,p}\}} a_2 J_m(c_{1h}^{k,n}, \bar{c}_{3h}^{k,n}, \tilde{\eta}_h^{k,n}) \mathbf{1}_{\Omega_m} \right) w_h \, dx = 0, \end{aligned} \quad (41)$$

$$\begin{aligned} & \int_{\Omega_2} \sigma \nabla \phi_{2h}^{k,n} \cdot \nabla v_h \, dx + \int_{\Omega_2} \left(\sum_{m \in \{\text{n,p}\}} a_2 J_m(c_{1h}^{k,n}, \bar{c}_{3h}^{k,n}, \tilde{\eta}_h^{k,n}) \mathbf{1}_{\Omega_m} \right) v_h \, dx \\ & + \int_{\Gamma} I^k v_h \, dx = 0, \end{aligned} \quad (42)$$

$$\begin{aligned} & \int_{\Omega_2} \int_0^{R_s(x)} \frac{c_{3h\Delta r}^{k,n} - c_{2h\Delta r}^{k-1}}{\tau} v_{h\Delta r} r^2 dr dx + \int_{\Omega_2} \int_0^{R_s(x)} k_2 \frac{\partial c_{3h\Delta r}^{k,n}}{\partial r} \frac{\partial v_{h\Delta r}}{\partial r} r^2 dr dx \\ & + \int_{\Omega_2} \left(\sum_{m \in \{n,p\}} \frac{R_s^2}{F} J_m(c_{1h}^{k,n}, \bar{c}_{3h}^{k,n}, \tilde{\eta}_h^{k,n}) \mathbf{1}_{\Omega_m} \right) v_{h\Delta r}(x, R_s(x)) dx = 0, \quad (43) \end{aligned}$$

where $\kappa_{ih}^{k,n} = \sum_{m \in \{n,s,p\}} \kappa_{im}(c_{1h}^{k,n}) \mathbf{1}_{\Omega_m}$, $i = 1, 2$, $\tilde{\eta}_h^{k,n} = \phi_{2h}^{k,n} - \phi_{1h}^{k,n} - \tilde{U}_h^{k,n}$, and $\tilde{U}_h^{k,n} = \sum_{m \in \{n,p\}} U_m(\bar{c}_{3h}^{k,n}) \mathbf{1}_{\Omega_m}$.

Step 3 (Subproblem (c₂)): Find $c_{2h\Delta r}^{k,n} \in V_{h\Delta r}(\bar{\Omega}_{2r})$, such that for all $v_{h\Delta r} \in V_{h\Delta r}(\bar{\Omega}_{2r})$,

$$\begin{aligned} & \int_{\Omega_2} \int_0^{R_s(x)} \frac{c_{2h\Delta r}^{k,n} - c_{2h\Delta r}^{k-1}}{\tau} v_{h\Delta r} r^2 dr dx + \int_{\Omega_2} \int_0^{R_s(x)} k_2 \frac{\partial c_{2h\Delta r}^{k,n}}{\partial r} \frac{\partial v_{h\Delta r}}{\partial r} r^2 dr dx \\ & + \int_{\Omega_2} \left(\sum_{m \in \{n,p\}} \frac{R_s^2}{F} J_m(c_{1h}^{k,n}, \bar{c}_{2h}^{k,n}, \eta_h^{k,n}) \mathbf{1}_{\Omega_m} \right) v_{h\Delta r}(x, R_s(x)) dx = 0. \quad (44) \end{aligned}$$

where $\eta_h^{k,n} = \phi_{2h}^{k,n} - \phi_{1h}^{k,n} - U_h^{k,n}$, and $U_h^{k,n} = \sum_{m \in \{n,p\}} U_m(\bar{c}_{2h}^{k,n}) \mathbf{1}_{\Omega_m}$.

Step 4: If $\frac{\|X^n - X^{n-1}\|}{\|X^{n-1}\|} < rtol$ for $X^n := (c_{1h}^{k,n}, \phi_{1h}^{k,n}, \phi_{2h}^{k,n}, c_{2h\Delta r}^{k,n})$, terminate the iteration, and set $\phi_{1h}^k = \phi_{1h}^{k,n}$, $\phi_{2h}^k = \phi_{2h}^{k,n}$, $c_{1h}^k = c_{1h}^{k,n}$, $c_{2h\Delta r}^k = c_{2h\Delta r}^{k,n}$. Otherwise, set $n = n + 1$ and return to **Step 1**.

Remark 3.1. Take $v_{h\Delta r}(x, r) = \chi_i(x) \psi_{N_i}(r)$, $i = 1, \dots, M_2$ as the trial functions in (43), and we have, for $\hat{e}_i \in \mathcal{T}_{h,m}$, $m \in \{n,p\}$,

$$\begin{aligned} & \int_0^{R_s(x)} \frac{c_{3h\Delta r,ij}^{k,n} - c_{2h\Delta r,ij}^{k-1}}{\tau} \psi_j \psi_{N_i} r^2 dr + \int_0^{R_s(x)} k_2 c_{3h\Delta r,ij}^{k,n} \frac{\partial \psi_j}{\partial r} \frac{\partial \psi_{N_i}}{\partial r} r^2 dr \\ & + \frac{1}{|\hat{e}_i|} \int_{\hat{e}_i} \left(\sum_{m \in \{n,p\}} \frac{R_s^2}{F} J_m(c_{1h}^{k,n}, \bar{c}_{3h}^{k,n}, \tilde{\eta}_h^{k,n}) \mathbf{1}_{\Omega_m} \right) dx = 0. \quad (45) \end{aligned}$$

From the definition (38), we can see that only $\bar{c}_{3h\Delta r}$ is coupled in **Step 2** and (43) is equivalent to the above M_2 x -independent 1D equations.

4. Numerical experiments

To validate the theoretical analysis and demonstrate the superiority of the solver proposed in this paper, we present numerical simulations for the DFN model using real battery parameters from [3, 16]. The simulations are implemented using an in-house finite element code based on the libMesh library [49].

4.1. Convergence validation

Due to computational resource limitations, complete validation of the convergence order for the P3D model is reported here while partial results for the P4D model can be found in Appendix B.

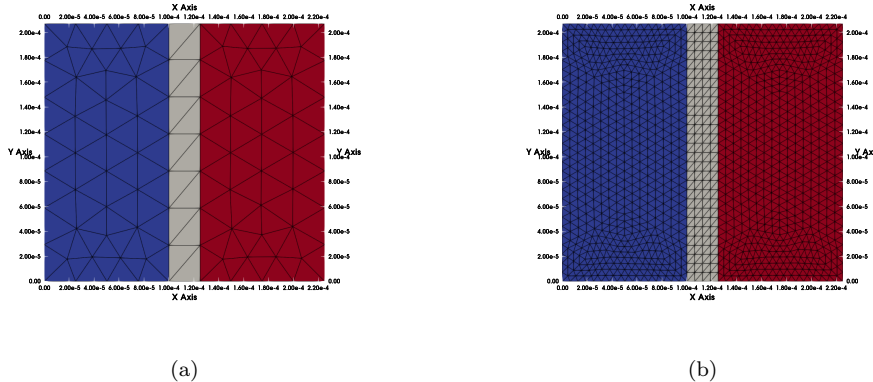


Figure 2: Spatial meshes for convergence verification. (a) Initial coarse mesh ($R_h = 0$). (b) Uniformly refined mesh ($R_h = 2$).

In this example, we set $\Omega_n = [0, 100] \times [0, 207]$, $\Omega_s = [100, 125] \times [0, 207]$, and $\Omega_p = [125, 225] \times [0, 207]$ (all dimensions in 10^{-6}m). The boundary Γ is defined as $\Gamma_n \cup \Gamma_p$, where $\Gamma_n = \{0\} \times [0, 207]$ and $\Gamma_p = \{225\} \times [0, 207]$. A 1C discharge rate is applied, using parameters from [16].

The initial spatial mesh, shown in Figure 2a, is refined uniformly with level R_h . The radial grid is initially uniform, with grid size $\Delta r = 1.25 \times 10^{-6}\text{m}$ and refinement level $R_{\Delta r}$. Since the exact solution is unknown, we use the finite element solution on a very fine mesh ($R_h = 5$, $R_{\Delta r} = 5$) with a sufficiently small step size $\tau_{\text{ref}} = 0.0390625\text{s}$ as a reference.

Figure 3 illustrates the absolute errors as a function of the time step size τ for all variables, evaluated at $T = 1.25\text{s}$ with $R_h = 5$ and $R_{\Delta r} = 5$ fixed.

For fixed $R_{\Delta r} = 5$ ($R_h = 5$) and $\tau = \tau_{\text{ref}}$, we refine the initial mesh from $R_h = 1$ ($R_{\Delta r} = 1$) to $R_h = 3$ ($R_{\Delta r} = 3$). The error and convergence order with respect to h (Δr) at time $t_k = k\Delta t$ are summarized in Table 1 (Table 2). The observed convergence rates agree with our theoretical analysis.

Table 1: Error and convergence order for h .

(a) $\ \phi_1(\cdot, t_k) - \phi_{1h}^k\ _{H^1(\Omega)}$					(b) $\ \phi_2(\cdot, t_k) - \phi_{2h}^k\ _{H^1(\Omega_2)}$				
k	$R_h = 1$	$R_h = 2$	$R_h = 3$	Order	k	$R_h = 1$	$R_h = 2$	$R_h = 3$	Order
2	9.90E-04	4.92E-04	2.40E-04	1.04	2	3.32E-05	1.65E-05	8.06E-06	1.03
4	9.90E-04	4.90E-04	2.39E-04	1.04	4	3.32E-05	1.65E-05	8.06E-06	1.03
6	1.02E-03	5.06E-04	2.47E-04	1.04	6	3.32E-05	1.65E-05	8.06E-06	1.03
8	1.06E-03	5.25E-04	2.56E-04	1.04	8	3.32E-05	1.65E-05	8.06E-06	1.03
10	1.05E-03	5.19E-04	2.53E-04	1.04	10	3.32E-05	1.65E-05	8.06E-06	1.03
(c) $\ c_1(\cdot, t_k) - c_{1h}^k\ _{H^1(\Omega)}$					(d) $\ \bar{c}_2(\cdot, t_k) - \bar{c}_{2h}^k\ _{L^2(\Omega_2)}$				
k	$R_h = 1$	$R_h = 2$	$R_h = 3$	Order	k	$R_h = 1$	$R_h = 2$	$R_h = 3$	Order
2	4.24E+00	2.25E+00	1.11E+00	1.02	2	1.36E-02	6.77E-03	3.31E-03	1.04
4	4.70E+00	2.37E+00	1.16E+00	1.03	4	2.96E-03	1.47E-03	7.18E-04	1.04
6	5.70E+00	2.89E+00	1.42E+00	1.03	6	7.91E-03	3.94E-03	1.92E-03	1.03
8	6.80E+00	3.42E+00	1.68E+00	1.03	8	1.73E-02	8.63E-03	4.21E-03	1.04
10	6.83E+00	3.40E+00	1.66E+00	1.04	10	1.21E-02	5.99E-03	2.92E-03	1.03
(e) $\ c_2(\cdot, t_k) - c_{2h\Delta r}^k\ _{L^2(\Omega_2; H_r^1(0, R_s(\cdot)))}$					(f) $\ c_2(\cdot, t_k) - c_{2h\Delta r}^k\ _{L^2(\Omega_2; L_r^2(0, R_s(\cdot)))}$				
k	$R_h = 1$	$R_h = 2$	$R_h = 3$	Order	k	$R_h = 1$	$R_h = 2$	$R_h = 3$	Order
2	2.45E-05	1.22E-05	5.94E-06	1.03	2	3.44E-12	1.71E-12	8.35E-13	1.04
4	9.85E-06	4.89E-06	2.39E-06	1.04	4	2.01E-12	9.97E-13	4.87E-13	1.04
6	1.16E-05	5.81E-06	2.84E-06	1.03	6	2.43E-12	1.21E-12	5.91E-13	1.03
8	2.71E-05	1.36E-05	6.62E-06	1.04	8	4.85E-12	2.42E-12	1.18E-12	1.04
10	1.86E-05	9.26E-06	4.52E-06	1.03	10	4.59E-12	2.28E-12	1.11E-12	1.03

4.2. Performance comparison

We compare the performance of the newly proposed algorithm (referred to as "Novel") with existing algorithms outlined in Appendix C (Macro, Potential, and Decouple). All nonlinear subproblems are solved exactly using Newton's method with an absolute iteration tolerance of 1e-14. The default

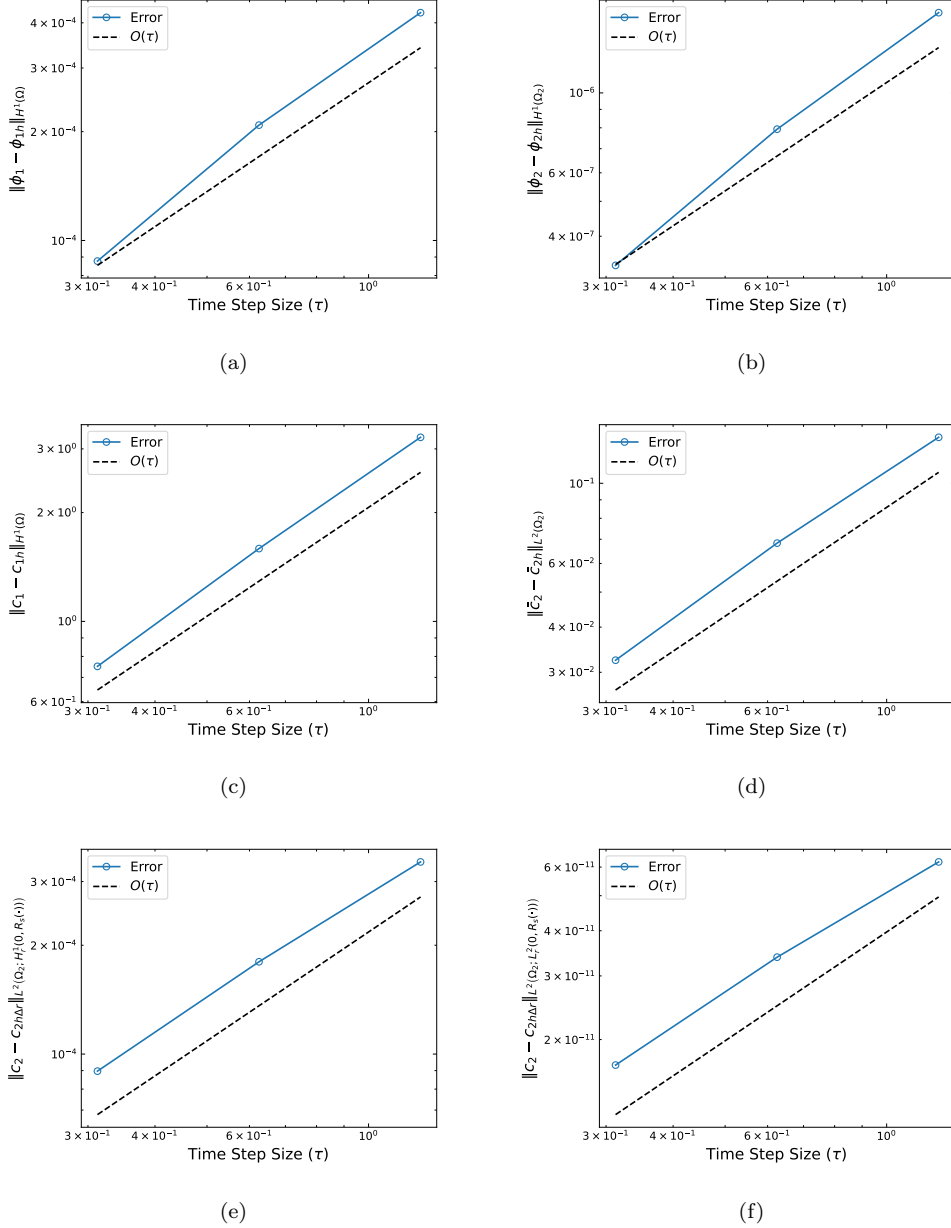


Figure 3: Time convergence obtained at $t = 1.25$ s. (a) Error for ϕ_1 in the H^1 -norm. (b) Error for ϕ_2 in the H^1 -norm. (c) Error for c_1 in the H^1 -norm. (d) Error for \bar{c}_2 in the L^2 -norm. (e) Error for c_2 in the $L^2(H_r^1)$ -norm. (f) Error for c_2 in the $L^2(L_r^2)$ -norm.

Table 2: Error and convergence order for r .

(a) $\ \phi_1(\cdot, t_k) - \phi_{1h}^k\ _{H^1(\Omega)}$					(b) $\ \phi_2(\cdot, t_k) - \phi_{2h}^k\ _{H^1(\Omega_2)}$				
k	$R_h = 1$	$R_h = 2$	$R_h = 3$	Order	k	$R_h = 1$	$R_h = 2$	$R_h = 3$	Order
2	1.33E-05	3.04E-06	7.09E-07	2.10	2	5.52E-08	1.28E-08	2.99E-09	2.10
4	1.86E-05	4.58E-06	1.08E-06	2.08	4	7.75E-08	1.89E-08	4.46E-09	2.08
6	5.07E-06	1.32E-06	3.15E-07	2.06	6	2.10E-08	5.40E-09	1.29E-09	2.07
8	2.60E-06	6.31E-07	1.50E-07	2.07	8	1.01E-08	2.44E-09	5.80E-10	2.07
10	4.99E-06	1.31E-06	3.14E-07	2.06	10	1.89E-08	4.98E-09	1.19E-09	2.06
(c) $\ c_1(\cdot, t_k) - c_{1h}^k\ _{H^1(\Omega)}$					(d) $\ \bar{c}_2(\cdot, t_k) - \bar{c}_{2h}^k\ _{L^2(\Omega_2)}$				
k	$R_h = 1$	$R_h = 2$	$R_h = 3$	Order	k	$R_h = 1$	$R_h = 2$	$R_h = 3$	Order
2	1.87E-02	4.34E-03	1.02E-03	2.10	2	4.20E-03	1.01E-03	2.38E-04	2.08
4	9.75E-03	2.49E-03	5.93E-04	2.07	4	1.94E-03	4.41E-04	1.05E-04	2.08
6	2.15E-03	5.88E-04	1.42E-04	2.05	6	1.38E-03	3.25E-04	7.74E-05	2.07
8	8.44E-03	2.03E-03	4.84E-04	2.07	8	1.08E-03	2.54E-04	6.05E-05	2.07
10	1.09E-02	2.75E-03	6.57E-04	2.07	10	9.64E-04	2.28E-04	5.44E-05	2.07
(e) $\ c_2(\cdot, t_k) - c_{2h\Delta r}^k\ _{L^2(\Omega_2; H_r^1(0, R_s(\cdot)))}$					(f) $\ c_2(\cdot, t_k) - c_{2h\Delta r}^k\ _{L^2(\Omega_2; L_r^2(0, R_s(\cdot)))}$				
k	$R_h = 1$	$R_h = 2$	$R_h = 3$	Order	k	$R_h = 1$	$R_h = 2$	$R_h = 3$	Order
2	1.72E-04	8.55E-05	4.17E-05	1.04	2	2.01E-12	5.02E-13	1.23E-13	2.04
4	1.33E-04	6.60E-05	3.22E-05	1.03	4	1.69E-12	4.26E-13	1.03E-13	2.04
6	1.09E-04	5.44E-05	2.65E-05	1.03	6	1.48E-12	3.71E-13	9.00E-14	2.04
8	9.85E-05	4.90E-05	2.39E-05	1.03	8	1.41E-12	3.52E-13	8.51E-14	2.05
10	8.94E-05	4.46E-05	2.18E-05	1.03	10	1.34E-12	3.35E-13	8.10E-14	2.05

line search type in PETSc [50] is employed to ensure robust convergence, and the linear system at each Newton step is solved using SuperLU_DIST [51], which is a distributed-memory sparse direct solver for large sets of linear equations.

Numerical results with different solution scales for the P4D model (see Appendix B), presented in Table 3, show that the novel solver outperforms its competitors, nearly doubling the speed of the second-fastest solver, the potential-coupled solver. While the fully decoupled solver is attractive due to its simplicity, it proves inefficient when the governing equations are strongly coupled. The results also indicate that a greater degree of coupling does not necessarily lead to higher efficiency, as demonstrated by the macroscale-coupled solver. Ultimately, the efficiency gains depend more on the understanding of the problem’s physics and the strength of the coupling between the governing equations.

A deeper analysis of the table data reveals that the newly proposed algorithm significantly accelerates the solution process, primarily due to a reduction in the number of outer iterations, as anticipated. Although the memory overhead increases with the introduction of more coupling, the memory overhead of our solver remains nearly the same as that of the potential-coupled solver. This is because of the piecewise-constant discretization of $\bar{c}_{3h}^{k,n}$, with only a few additional nonzero entries added to the Jacobian.

Table 3: Performance Comparison Table

(a) Parallel running time (hours)					(b) Total CPU time (hours)				
#Nodes	Decouple	Potential	Novel	Macro	#Nodes	Decouple	Potential	Novel	Macro
1331	0.53	0.12	0.07	0.17	1331	132.92	25.52	16.80	42.05
9261	2.55	0.55	0.35	1.18	9261	641.54	132.25	87.68	294.84
68921	24.69	4.26	2.57	9.72	68921	6205.02	1065.38	645.05	2441.97
531441	226.34	46.61	28.47	175.40	531441	56880.07	11708.96	7152.71	44079.42
(c) Average number of outer iterations					(d) Average memory usage (GB)				
#Nodes	Decouple	Potential	Novel	Macro	#Nodes	Decouple	Potential	Novel	Macro
1331	39	6	3	6	1331	15.66	13.84	10.13	13.58
9261	36	6	3	6	9261	21.23	21.86	21.05	23.49
68921	39	6	3	6	68921	51.80	58.73	60.02	75.02
531441	40	6	3	6	531441	257.67	319.24	339.56	417.53

5. Conclusions

In this paper, we present the error analysis of a backward Euler finite element discretization for the DFN model of lithium-ion batteries. We establish the optimal convergence rate in N -dimensions ($1 \leq N \leq 3$). Furthermore, we propose a novel and efficient solver that accelerates computation while maintaining low memory requirements. Numerical experiments using real battery parameters validate our theoretical results and demonstrate that the proposed algorithm is the most cost-effective among existing scale-decoupled algorithms.

Appendix A. Function spaces and notations

Let $H^m(\Omega)$ ($m \in \mathbb{N}_0$) denote the Sobolev spaces $W^{m,2}(\Omega)$ defined on a generic bounded domain Ω with the norm $\|\cdot\|_{m,\Omega} = \|\cdot\|_{W^{m,2}(\Omega)}$. We also denote the subspace of $H^1(\Omega)$, consisting of functions whose integral is zero, by

$$H_*^1(\Omega) := \left\{ v \in H^1(\Omega) : \int_{\Omega} v \, dx = 0 \right\}.$$

Since multiple domains Ω_n , Ω_s and Ω_p are involved, it is necessary to further define piecewise Sobolev spaces

$$H_{\text{pw}}^m(\Omega_1) = H^m(\Omega_n) \cap H^m(\Omega_s) \cap H^m(\Omega_p)$$

equipped with the norm $\|\cdot\|_{m,\Omega_1} := \|\cdot\|_{m,\Omega_n} + \|\cdot\|_{m,\Omega_s} + \|\cdot\|_{m,\Omega_p}$, and

$$H_{\text{pw}}^m(\Omega_2) = H^m(\Omega_n) \cap H^m(\Omega_p)$$

with $\|\cdot\|_{m,\Omega_2} := \|\cdot\|_{m,\Omega_n} + \|\cdot\|_{m,\Omega_p}$.

The natural space for radial solutions with radial coordinate r is $L_r^2(0, R)$, consisting of measurable functions v defined on $(0, R)$ such that vr is L^2 -integrable. It is obvious that $L_r^2(0, R)$ is a Hilbert space and can be endowed with the norm

$$\|v\|_{L_r^2(0,R)} = \left(\int_0^R |v(r)|^2 r^2 \, dr \right)^{\frac{1}{2}}.$$

We also denote by $H_r^m(0, R)$ ($m \in \mathbb{N}_0$) the Hilbert spaces of measurable functions v , whose distribution derivatives belong to $L_r^2(0, R)$ up to order m , with the norm

$$\|v\|_{H_r^m(0,R)} = \left(\sum_{k=0}^m \left\| \frac{d^k v}{dr^k} \right\|_{L_r^2(0,R)}^2 \right)^{\frac{1}{2}}. \quad (\text{A.1})$$

For functions in $H_r^1(0, R)$, we have the following critical trace estimation in [22]:

Proposition Appendix A.1. *There exist an arbitrarily small number ϵ and a positive (possibly large) constant $C(\epsilon)$, such that for $u \in H_r^1(0, R)$,*

$$|u(R)| \leq \epsilon \left\| \frac{\partial u}{\partial r} \right\|_{L_r^2(0,R)} + C(\epsilon) \|u\|_{L_r^2(0,R)}.$$

Let X be a Banach space. Vector-valued Lebesgue spaces $L^p(\Omega; X)$, $1 \leq p \leq \infty$, and Sobolev spaces $H^m(\Omega; X)$, $m \in \mathbb{N}_0$, for a generic domain Ω are introduced. It is convenient for c_2 with Ω_2 and R_s in Section 1 to define

$$H^p(\Omega_2; H_r^q(0, R_s(\cdot))) := H^p(\Omega_n; H_r^q(0, R_n)) \cap H^p(\Omega_p; H_r^q(0, R_p)), \quad p, q \in \mathbb{N}_0,$$

with the norm $\|\cdot\|_{p, \Omega_2; q, r} = \|\cdot\|_{H^p(\Omega_n; H_r^q(0, R_n))} + \|\cdot\|_{H^p(\Omega_p; H_r^q(0, R_p))}$. Besides, for time-dependent variables with $\Omega = [0, T]$, notations $(H^m(0, T; X), \|\cdot\|_{m; X})$ are used, and for a partition of the interval $[0, T]$, $0 = t_0 < t_1 < \dots < t_M = T$, we define $\|\cdot\|_{0, k; X} := \left(\int_{t_{k-1}}^{t_k} \|\cdot\|_X^2 dt \right)^{\frac{1}{2}}$, $k = 1, 2, \dots, M$.

Appendix B. Numerical error and order in 3D

In this example, we set $\Omega_n = [0, 50] \times [0, 111.8] \times [0, 111.8]$, $\Omega_s = [50, 75.4] \times [0, 111.8] \times [0, 111.8]$, and $\Omega_p = [75.4, 111.8] \times [0, 111.8] \times [0, 111.8]$ (all dimensions in 10^{-6}m). The boundary Γ is defined as $\Gamma_n \cup \Gamma_p$, where $\Gamma_n = \{0\} \times [0, 111.8] \times [0, 111.8]$ and $\Gamma_p = \{111.8\} \times [0, 111.8] \times [0, 111.8]$. A 5C (30A) discharge rate is applied, using parameters from [3].

The initial spatial mesh is shown by Figure B.4 and the initial radial grid is uniform with the grid size $\Delta r = 1.25 \times 10^{-7}\text{m}$. The finite element solution in an extremely fine mesh ($R_h = 5$ and $R_{\Delta r} = 5$) with a sufficiently small step size $\tau_{\text{ref}} = 0.15625\text{s}$ is taken as the reference solution.

Fixing $R_h = 5$, $R_{\Delta r} = 5$ and refining the initial time step size twice, the convergence error and order of all numerical solutions with respect to τ at $T = 2.5\text{ s}$ are presented in Table B.4. Fixing $R_{\Delta r} = 5$, $\tau = \tau_{\text{ref}}$ and refining the initial spatial mesh twice, the convergence error and order with respect to h at $t_k = k\tau$ are presented in Table B.5. We can clearly see the convergence rates $\mathcal{O}(\tau)$ and $\mathcal{O}(h)$, which agree with our analysis.

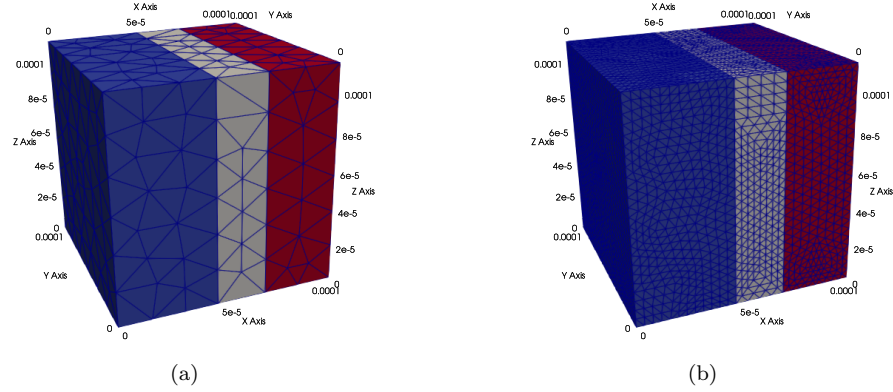


Figure B.4: Spatial meshes for convergence verification. (a) Initial coarse mesh ($R_h = 0$).
 (b) Uniformly refined mesh ($R_h = 2$).

Table B.4: Error and convergence order for τ .

$t_k = 2.5[s]$	$R_\tau = 0$	$R_\tau = 1$	$R_\tau = 2$	Order
$\ c_1(\cdot, t_k) - c_{1h}^k\ _{H^1}$	1.08E-01	5.17E-02	2.32E-02	1.16
$\ \bar{c}_2(\cdot, t_k) - \bar{c}_{2h}^k\ _{L^2}$	3.04E-01	1.40E-01	6.07E-02	1.21
$\ \phi_1(\cdot, t_k) - \phi_{1h}^k\ _{H^1}$	3.28E-06	1.44E-06	6.46E-07	1.15
$\ \phi_2(\cdot, t_k) - \phi_{2h}^k\ _{H^1}$	3.22E-08	2.92E-09	1.32E-09	1.15

Table B.5: Error and convergence order for h .

(a) $\ \phi_1(\cdot, t_k) - \phi_{1h}^k\ _{H^1(\Omega)}$					(b) $\ \phi_2(\cdot, t_k) - \phi_{2h}^k\ _{H^1(\Omega_2)}$				
k	$R_h = 0$	$R_h = 1$	$R_h = 2$	Order	k	$R_h = 0$	$R_h = 1$	$R_h = 2$	Order
1	4.48E-06	2.51E-06	1.29E-06	0.96	1	7.40E-07	3.75E-07	1.85E-07	1.02
16	9.48E-06	4.85E-06	2.39E-06	1.02	16	7.40E-07	3.75E-07	1.85E-07	1.02
32	1.20E-05	6.06E-06	2.98E-06	1.02	32	7.40E-07	3.75E-07	1.85E-07	1.02
64	1.50E-05	7.57E-06	3.72E-06	1.02	64	7.40E-07	3.75E-07	1.85E-07	1.02
(c) $\ c_1(\cdot, t_k) - c_{1h}^k\ _{H^1(\Omega)}$					(d) $\ \bar{c}_2(\cdot, t_k) - \bar{c}_{2h}^k\ _{L^2(\Omega_2)}$				
k	$R_h = 0$	$R_h = 1$	$R_h = 2$	Order	k	$R_h = 0$	$R_h = 1$	$R_h = 2$	Order
1	7.29E-02	4.94E-02	2.70E-02	0.87	1	5.29E-01	2.93E-01	1.49E-01	0.97
16	2.46E-01	1.27E-01	6.25E-02	1.02	16	1.32E+00	6.76E-01	3.33E-01	1.02
32	3.26E-01	1.66E-01	8.16E-02	1.02	32	1.51E+00	7.66E-01	3.77E-01	1.02
64	4.26E-01	2.16E-01	1.06E-01	1.02	64	1.56E+00	7.90E-01	3.88E-01	1.02

Appendix C. Scale-decoupled solvers in the literature

Here, we provide a comprehensive list of all scale-decoupled solvers available in the literature to the best of our knowledge, whose performance is compared in Subsection 4.2.

Let $(\phi_{1h}^{k-1}, \phi_{2h}^{k-1}, c_{1h}^{k-1}, c_{2h\Delta r}^{k-1})$ be the fully discrete solution of the $(k-1)$ -th time step. We focus on solving for the solution at the k -th time step, $(\phi_{1h}^k, \phi_{2h}^k, c_{1h}^k, c_{2h\Delta r}^k)$. All solvers considered here follow the same initialization and termination procedures outlined in Section 3.

Appendix C.1. Macroscale-coupled solver [42]

Step 1 (Subproblem (c_1, ϕ_1, ϕ_2)): Find $c_{1h}^{k,n} \in V_h^{(1)}(\bar{\Omega})$, $\phi_{1h}^{k,n} \in W_h(\bar{\Omega})$ and $\phi_{2h}^{k,n} \in V_h^{(1)}(\bar{\Omega}_2)$, such that for all $v_{1h} \in V_h^{(1)}(\bar{\Omega})$, $w_h \in W_h(\bar{\Omega})$ and $v_{2h} \in V_h^{(1)}(\bar{\Omega}_2)$,

$$\begin{aligned} & \int_{\Omega} \varepsilon_1 \frac{c_{1h}^{k,n} - c_{1h}^{k-1}}{\tau} v_{1h} \, dx + \int_{\Omega} k_1 \nabla c_{1h}^{k,n} \cdot \nabla v_{1h} \, dx \\ & - \int_{\Omega_2} \left(\sum_{m \in \{n, p\}} a_1 J_m(c_{1h}^{k,n}, \bar{c}_{2h}^{k,n-1}, \tilde{\eta}_h^{k,n}) \mathbf{1}_{\Omega_m} \right) v_{1h} \, dx = 0, \quad (\text{C.1}) \end{aligned}$$

$$\begin{aligned} & \int_{\Omega} \kappa_{1h}^{k,n} \nabla \phi_{1h}^k \cdot \nabla w_h \, dx - \int_{\Omega} \kappa_{2h}^{k,n} \nabla f\left(c_{1h}^{k,n}\right) \cdot \nabla w_h \, dx \\ & - \int_{\Omega_2} \left(\sum_{m \in \{\text{n,p}\}} a_2 J_m\left(c_{1h}^{k,n}, \bar{c}_{2h}^{k,n-1}, \tilde{\eta}_h^{k,n}\right) \mathbf{1}_{\Omega_m} \right) w_h \, dx = 0, \quad (\text{C.2}) \end{aligned}$$

$$\begin{aligned} & \int_{\Omega_2} \sigma \nabla \phi_{2h}^{k,n} \cdot \nabla v_{2h} \, dx + \int_{\Omega_2} \left(\sum_{m \in \{\text{n,p}\}} a_2 J_m\left(c_{1h}^{k,n}, \bar{c}_{2h}^{k,n-1}, \tilde{\eta}_h^{k,n}\right) \mathbf{1}_{\Omega_m} \right) v_{2h} \, dx \\ & + \int_{\Gamma} I^k v_{2h} \, dx = 0, \quad (\text{C.3}) \end{aligned}$$

where $\kappa_{ih}^{k,n} = \sum_{m \in \{\text{n,s,p}\}} \kappa_{im}\left(c_{1h}^{k,n}\right) \mathbf{1}_{\Omega_m}$, $i = 1, 2$ and $\tilde{\eta}_h^{k,n} = \phi_{2h}^{k,n} - \phi_{1h}^{k,n} - U_h^{k,m-1}$.

Step 2 (Subproblem c_2): Find $c_{2h\Delta r}^{k,n} \in V_{h\Delta r}(\bar{\Omega}_{2r})$, such that for all $v_{h\Delta r} \in V_{h\Delta r}(\bar{\Omega}_{2r})$,

$$\begin{aligned} & \int_{\Omega_2} \int_0^{R_s(x)} \frac{c_{2h\Delta r}^{k,n} - c_{2h\Delta r}^{k-1}}{\tau} v_{h\Delta r} r^2 \, dr \, dx + \int_{\Omega_2} \int_0^{R_s(x)} k_2 \frac{\partial c_{2h\Delta r}^{k,n}}{\partial r} \frac{\partial v_{h\Delta r}}{\partial r} r^2 \, dr \, dx \\ & + \int_{\Omega_2} \left(\sum_{m \in \{\text{n,p}\}} \frac{R_s^2}{F} J_m\left(c_{1h}^{k,n}, \bar{c}_{2h}^{k,n}, \eta_h^{k,n}\right) \mathbf{1}_{\Omega_m} \right) v_{h\Delta r}(x, R_s(x)) \, dx = 0, \quad (\text{C.4}) \end{aligned}$$

where $\eta_h^{k,n} = \phi_{2h}^{k,n} - \phi_{1h}^{k,n} - U_h^{k,n}$, and $U_h^{k,n} = \sum_{m \in \{\text{n,p}\}} U_m(\bar{c}_{2h}^{k,n}) \mathbf{1}_{\Omega_m}$.

Appendix C.2. Potential-coupled solver [13]

Step 1 (Subproblem c_1): Find $c_{1h}^{k,n} \in V_h^{(1)}(\bar{\Omega})$, such that for all $v_h \in V_h^{(1)}(\bar{\Omega})$,

$$\begin{aligned} & \int_{\Omega} \varepsilon_1 \frac{c_{1h}^{k,n} - c_{1h}^{k-1}}{\tau} v_h \, dx + \int_{\Omega} k_1 \nabla c_{1h}^{k,n} \cdot \nabla v_h \, dx \\ & - \int_{\Omega_2} \left(\sum_{m \in \{\text{n,p}\}} a_1 J_m\left(c_{1h}^{k,n}, \bar{c}_{2h}^{k,n-1}, \eta_h^{k,n-1}\right) \mathbf{1}_{\Omega_m} \right) v_h \, dx = 0. \quad (\text{C.5}) \end{aligned}$$

Step 2 (Subproblem (ϕ_1, ϕ_2)): Find $\phi_{1h}^{k,n} \in W_h(\bar{\Omega})$, $\phi_{2h}^{k,n} \in V_h^{(1)}(\bar{\Omega}_2)$, such that for all $w_h \in W_h(\bar{\Omega})$, $v_h \in V_h^{(1)}(\bar{\Omega}_2)$,

$$\begin{aligned} & \int_{\Omega} \kappa_{1h}^{k,n} \nabla \phi_{1h}^k \cdot \nabla w_h \, dx - \int_{\Omega} \kappa_{2h}^{k,n} \nabla f(c_{1h}^{k,n}) \cdot \nabla w_h \, dx \\ & - \int_{\Omega_2} \left(\sum_{m \in \{n, p\}} a_2 J_m(c_{1h}^{k,n}, \bar{c}_{2h}^{k,n-1}, \tilde{\eta}_h^{k,n}) \mathbf{1}_{\Omega_m} \right) w_h \, dx = 0, \quad (\text{C.6}) \end{aligned}$$

$$\begin{aligned} & \int_{\Omega_2} \sigma \nabla \phi_{2h}^{k,n} \cdot \nabla v_h \, dx + \int_{\Omega_2} \left(\sum_{m \in \{n, p\}} a_2 J_m(c_{1h}^{k,n}, \bar{c}_{2h}^{k,n-1}, \tilde{\eta}_h^{k,n}) \mathbf{1}_{\Omega_m} \right) v_h \, dx \\ & + \int_{\Gamma} I^k v_h \, dx = 0, \quad (\text{C.7}) \end{aligned}$$

where $\kappa_{ih}^{k,n} = \sum_{m \in \{n, s, p\}} \kappa_{im}(c_{1h}^{k,n}) \mathbf{1}_{\Omega_m}$, $i = 1, 2$, $\tilde{\eta}_h^{k,n} = \phi_{2h}^{k,n} - \phi_{1h}^{k,n} - U_h^{k,n-1}$.

Step 3 (Subproblem c_2): Find $c_{2h\Delta r}^{k,n} \in V_{h\Delta r}(\bar{\Omega}_{2r})$, such that for all $v_{h\Delta r} \in V_{h\Delta r}(\bar{\Omega}_{2r})$,

$$\begin{aligned} & \int_{\Omega_2} \int_0^{R_s(x)} \frac{c_{2h\Delta r}^{k,n} - c_{2h\Delta r}^{k-1}}{\tau} v_{h\Delta r} r^2 \, dr \, dx + \int_{\Omega_2} \int_0^{R_s(x)} k_2 \frac{\partial c_{2h\Delta r}^{k,n}}{\partial r} \frac{\partial v_{h\Delta r}}{\partial r} r^2 \, dr \, dx \\ & + \int_{\Omega_2} \left(\sum_{m \in \{n, p\}} \frac{R_s^2}{F} J_m(c_{1h}^{k,n}, \bar{c}_{2h}^{k,n}, \eta_h^{k,n}) \mathbf{1}_{\Omega_m} \right) v_{h\Delta r}(x, R_s(x)) \, dx = 0, \quad (\text{C.8}) \end{aligned}$$

where $\eta_h^{k,n} = \phi_{2h}^{k,n} - \phi_{1h}^{k,n} - U_h^{k,n}$, and $U_h^{k,n} = \sum_{m \in \{n, p\}} U_m(\bar{c}_{2h}^{k,n}) \mathbf{1}_{\Omega_m}$.

Appendix C.3. Fully decoupled solver [39]

Step 1 (Subproblem c_2): Find $c_{2h\Delta r}^{k,n} \in V_{h\Delta r}(\bar{\Omega}_{2r})$, such that for all $v_{h\Delta r} \in V_{h\Delta r}(\bar{\Omega}_{2r})$,

$$\begin{aligned} & \int_{\Omega_2} \int_0^{R_s(x)} \frac{c_{2h\Delta r}^{k,n} - c_{2h\Delta r}^{k-1}}{\tau} v_{h\Delta r} r^2 \, dr \, dx + \int_{\Omega_2} \int_0^{R_s(x)} k_2 \frac{\partial c_{2h\Delta r}^{k,n}}{\partial r} \frac{\partial v_{h\Delta r}}{\partial r} r^2 \, dr \, dx \\ & + \int_{\Omega_2} \left(\sum_{m \in \{n, p\}} \frac{R_s^2}{F} J_m(c_{1h}^{k,n-1}, \bar{c}_{2h}^{k,n}, \tilde{\eta}_h^{k,n}) \mathbf{1}_{\Omega_m} \right) v_{h\Delta r}(x, R_s(x)) \, dx = 0, \end{aligned}$$

where $\tilde{\eta}_h^{k,n} = \phi_{2h}^{k,n-1} - \phi_{1h}^{k,n-1} - U_h^{k,n}$, and $U_h^{k,n} = \sum_{m \in \{n,p\}} U_m(\bar{c}_{2h}^{k,n}) \mathbf{1}_{\Omega_m}$.

Step 2 (Subproblem ϕ_2): Find $\phi_{2h}^{k,n} \in V_h^{(1)}(\bar{\Omega}_2)$, such that for all $v_h \in V_h^{(1)}(\bar{\Omega}_2)$,

$$\begin{aligned} & \int_{\Omega_2} \sigma \nabla \phi_{2h}^{k,n} \cdot \nabla v_h \, dx + \int_{\Omega_2} \left(\sum_{m \in \{n,p\}} a_2 J_m(c_{1h}^{k,n}, \bar{c}_{2h}^{k,n-1}, \tilde{\eta}_h^{k,n}) \mathbf{1}_{\Omega_m} \right) v_h \, dx \\ & \quad + \int_{\Gamma} I^k v_h \, dx = 0, \end{aligned}$$

where $\tilde{\eta}_h^{k,n} = \phi_{2h}^{k,n} - \phi_{1h}^{k,n-1} - U_h^{k,n}$.

Step 3 (Subproblem ϕ_1): Find $\phi_{1h}^{k,n} \in W_h(\bar{\Omega})$, such that for all $w_h \in W_h(\bar{\Omega})$,

$$\begin{aligned} & \int_{\Omega} \kappa_{1h}^{k,n-1} \nabla \phi_{1h}^k \cdot \nabla w_h \, dx - \int_{\Omega} \kappa_{2h}^{k,n-1} \nabla f(c_{1h}^{k,n-1}) \cdot \nabla w_h \, dx \\ & \quad - \int_{\Omega_2} \left(\sum_{m \in \{n,p\}} a_2 J_m(c_{1h}^{k,n-1}, \bar{c}_{2h}^{k,n}, \eta_h^{k,n}) \mathbf{1}_{\Omega_m} \right) w_h \, dx = 0, \quad (\text{C.9}) \end{aligned}$$

where $\eta_h^{k,n} = \phi_{2h}^{k,n} - \phi_{1h}^{k,n} - U_h^{k,n}$.

Step 4 (Subproblem c_1): Find $c_{1h}^{k,n} \in V_h^{(1)}(\bar{\Omega})$, such that for all $v_h \in V_h^{(1)}(\bar{\Omega})$,

$$\begin{aligned} & \int_{\Omega} \varepsilon_1 \frac{c_{1h}^{k,n} - c_{1h}^{k-1}}{\tau} v_h \, dx + \int_{\Omega} k_1 \nabla c_{1h}^{k,n} \cdot \nabla v_h \, dx \\ & \quad - \int_{\Omega_2} \left(\sum_{m \in \{n,p\}} a_1 J_m(c_{1h}^{k,n}, \bar{c}_{2h}^{k,n}, \eta_h^{k,n}) \mathbf{1}_{\Omega_m} \right) v_h \, dx = 0. \end{aligned}$$

References

- [1] M. Doyle, T. F. Fuller, J. Newman, Modeling of galvanostatic charge and discharge of the lithium/polymer/insertion cell, Journal of The Electrochemical Society 140 (1993) 1526–1533. doi:10.1149/1.2221597.

- [2] T. F. Fuller, M. Doyle, J. Newman, Simulation and optimization of the dual lithium ion insertion cell, *Journal of The Electrochemical Society* 141 (1994) 1–10. URL: <https://iopscience.iop.org/article/10.1149/1.2054684>. doi:10.1149/1.2054684.
- [3] K. Smith, C.-Y. Wang, Solid-state diffusion limitations on pulse operation of a lithium ion cell for hybrid electric vehicles, *Journal of Power Sources* 161 (2006) 628–639. doi:10.1016/j.jpowsour.2006.03.050.
- [4] V. Ramadesigan, P. W. C. Northrop, S. De, S. Santhanagopalan, R. D. Braatz, V. R. Subramanian, Modeling and simulation of lithium-ion batteries from a systems engineering perspective, *Journal of The Electrochemical Society* 159 (2012) R31. URL: <https://iopscience.iop.org/article/10.1149/2.018203jes/meta>. doi:10.1149/2.018203jes.
- [5] S. Shi, J. Gao, Y. Liu, Y. Zhao, Q. Wu, W. Ju, C. Ouyang, R. Xiao, Multi-scale computation methods: Their applications in lithium-ion battery research and development, *Chinese Physics B* 25 (2015) 018212.
- [6] G. L. Plett, *Battery Management Systems*, volume 1, Artech House, Boston, 2015.
- [7] T. Telmasre, N. Goswami, A. Concepción, S. Kolluri, M. Pathak, G. Morrison, V. R. Subramanian, Impedance response simulation strategies for lithium-ion battery models, *Current Opinion in Electrochemistry* 36 (2022) 101140. URL: <https://linkinghub.elsevier.com/retrieve/pii/S2451910322002058>. doi:10.1016/j.coelec.2022.101140.
- [8] L. Wu, Z. Lyu, Z. Huang, C. Zhang, C. Wei, Physics-based battery SOC estimation methods: Recent advances and future perspectives, *Journal of Energy Chemistry* 89 (2024) 27–40. URL: <https://linkinghub.elsevier.com/retrieve/pii/S209549562300565X>. doi:10.1016/j.jecchem.2023.09.045.
- [9] S. Golmon, K. Maute, M. L. Dunn, Multiscale design optimization of lithium ion batteries using adjoint sensitivity analysis, *International Journal for Numerical Methods in Engineering* 92 (2012) 475–494. URL: <https://onlinelibrary.wiley.com/doi/>

[abs/10.1002/nme.4347](https://doi.org/10.1002/nme.4347). doi:<https://doi.org/10.1002/nme.4347>.
[arXiv:https://onlinelibrary.wiley.com/doi/pdf/10.1002/nme.4347](https://onlinelibrary.wiley.com/doi/pdf/10.1002/nme.4347).

- [10] K. S. Hariharan, P. Tagade, S. Ramachandran, Mathematical Modeling of Lithium Batteries, Springer International Publishing, Cham, 2018. URL: <http://link.springer.com/10.1007/978-3-319-03527-7>. doi:10.1007/978-3-319-03527-7.
- [11] Z. Chen, D. L. Danilov, R.-A. Eichel, P. H. L. Notten, Porous Electrode Modeling and its Applications to Li-Ion Batteries, Advanced Energy Materials 12 (2022) 2201506. URL: <https://onlinelibrary.wiley.com/doi/abs/10.1002/aenm.202201506>. doi:10.1002/aenm.202201506.
- [12] F. B. Planella, W. Ai, A. M. Boyce, A. Ghosh, I. Korotkin, S. Sahu, V. Sulzer, R. Timms, T. G. Tranter, M. Zyskin, S. J. Cooper, J. S. Edge, J. M. Foster, M. Marinescu, B. Wu, G. Richardson, A continuum of physics-based lithium-ion battery models reviewed, Progress in Energy 4 (2022) 042003. URL: <https://dx.doi.org/10.1088/2516-1083/ac7d31>. doi:10.1088/2516-1083/ac7d31.
- [13] R. Bermejo, P. G. d. Sastre, An implicit-explicit Runge-Kutta-Chebyshev finite element method for the nonlinear Lithium-ion battery equations, Applied Mathematics and Computation 361 (2019) 398–420. doi:10.1016/j.amc.2019.05.011.
- [14] F. Ciucci, W. Lai, Derivation of micro/macro lithium battery models from homogenization, Transport in Porous Media 88 (2011) 249–270. doi:10.1007/s11242-011-9738-5.
- [15] H. Arunachalam, S. Onori, I. Battiato, On veracity of macroscopic Lithium-ion battery models, Journal of The Electrochemical Society 162 (2015) A1940. URL: <https://iopscience.iop.org/article/10.1149/2.0771509jes/meta>. doi:10.1149/2.0771509jes.
- [16] R. Timms, S. G. Marquis, V. Sulzer, C. P. Please, S. J. Chapman, Asymptotic reduction of a Lithium-ion pouch cell model, SIAM Journal on Applied Mathematics 81 (2021) 765–788. doi:10.1137/20M1336898.

- [17] G. W. Richardson, J. M. Foster, R. Ranom, C. P. Please, A. M. Ramos, Charge transport modelling of Lithium-ion batteries, *European Journal of Applied Mathematics* 33 (2022) 983–1031. doi:10.1017/S0956792521000292.
- [18] S. Xu, L. Cao, Optimal convergence in finite element semi-discrete error analysis of the Doyle-Fuller-Newman model beyond 1d with a novel projection operator, 2024. URL: <https://arxiv.org/abs/2411.10758>. arXiv:2411.10758.
- [19] C. Kroener, A mathematical exploration of a PDE system for lithium-ion batteries, Ph.D. thesis, UC Berkeley, 2016.
- [20] J. I. Díaz, D. Gómez-Castro, A. M. Ramos, On the well-posedness of a multiscale mathematical model for Lithium-ion batteries, *Advances in Nonlinear Analysis* 8 (2019) 1132–1157. doi:10.1515/anona-2018-0041.
- [21] L. Cai, R. E. White, Lithium ion cell modeling using orthogonal collocation on finite elements, *Journal of Power Sources* 217 (2012) 248–255. URL: <https://linkinghub.elsevier.com/retrieve/pii/S0378775312010439>. doi:10.1016/j.jpowsour.2012.06.043.
- [22] R. Bermejo, Numerical analysis of a finite element formulation of the P2D model for Lithium-ion cells, *Numerische Mathematik* 149 (2021) 463–505. doi:10.1007/s00211-021-01235-2.
- [23] J. S. Newman, N. P. Balsara, Electrochemical systems, fourth edition ed., Wiley, Hoboken, NJ, 2019.
- [24] Z. Mao, R. E. White, A finite-difference method for pseudo-two-dimensional boundary value problems, *Journal of The Electrochemical Society* 141 (1994) 151. URL: <https://iopscience.iop.org/article/10.1149/1.2054675/meta>. doi:10.1149/1.2054675.
- [25] G. S. Nagarajan, J. W. V. Zee, R. M. Spotnitz, A mathematical model for intercalation electrode behavior: I. Effect of particle-size distribution on discharge capacity, *Journal of The Electrochemical Society* 145 (1998) 771. URL: <https://iopscience.iop.org/article/10.1149/1.1838344/meta>. doi:10.1149/1.1838344.

- [26] Y. Zeng, P. Albertus, R. Klein, N. Chaturvedi, A. Kojic, M. Z. Bazant, J. Christensen, Efficient conservative numerical schemes for 1D nonlinear spherical diffusion equations with applications in battery modeling, *Journal of The Electrochemical Society* 160 (2013) A1565–A1571. URL: <https://iopscience.iop.org/article/10.1149/2.102309jes>. doi:10.1149/2.102309jes.
- [27] S. Mazumder, J. Lu, Faster-than-real-time simulation of lithium ion batteries with full spatial and temporal resolution, *International Journal of Electrochemistry* 2013 (2013) 1–10. doi:10.1155/2013/268747.
- [28] P. W. C. Northrop, V. Ramadesigan, S. De, V. R. Subramanian, Coordinate transformation, orthogonal collocation, model reformulation and simulation of electrochemical-thermal behavior of lithium-ion battery stacks, *Journal of The Electrochemical Society* 158 (2011) A1461. URL: <https://iopscience.iop.org/article/10.1149/2.058112jes/meta>. doi:10.1149/2.058112jes.
- [29] P. W. C. Northrop, M. Pathak, D. Rife, S. De, S. Santhanagopalan, V. R. Subramanian, Efficient simulation and model reformulation of two-dimensional electrochemical thermal behavior of lithium-ion batteries, *Journal of The Electrochemical Society* 162 (2015) A940–A951. URL: <https://iopscience.iop.org/article/10.1149/2.0341506jes>. doi:10.1149/2.0341506jes.
- [30] S. Kosch, Y. Zhao, J. Sturm, J. Schuster, G. Mulder, E. Ayerbe, A. Jossen, A computationally efficient multi-scale model for lithium-ion cells, *Journal of The Electrochemical Society* 165 (2018) A2374–A2388. URL: <https://iopscience.iop.org/article/10.1149/2.1241810jes>. doi:10.1149/2.1241810jes.
- [31] K. E. Brenan, S. L. Campbell, L. R. Petzold, Numerical Solution of Initial-Value Problems in Differential-Algebraic Equations, Society for Industrial and Applied Mathematics, Philadelphia, 1995. URL: <http://pubs.siam.org/doi/book/10.1137/1.9781611971224>. doi:10.1137/1.9781611971224.
- [32] I. Korotkin, S. Sahu, S. O’Kane, G. Richardson, J. M. Foster, Dan-deLiion v1: An extremely fast solver for the Newman model of

- lithium-ion battery (dis)charge, *Journal of The Electrochemical Society* 168 (2021) 060544. URL: <http://arxiv.org/abs/2102.06534>. doi:10.1149/1945-7111/ac085f.
- [33] T. Wickramanayake, M. Javadipour, K. Mehran, A Novel Solver for an Electrochemical–Thermal Ageing Model of a Lithium-Ion Battery, *Batteries* 10 (2024) 126. URL: <https://www.mdpi.com/2313-0105/10/4/126>. doi:10.3390/batteries10040126, number: 4 Publisher: Multidisciplinary Digital Publishing Institute.
 - [34] R. C. Aylagas, C. Gánuza, R. Parra, M. Yáñez, E. Ayerbe, cide-MOD: An Open Source Tool for Battery Cell Inhomogeneous Performance Understanding, *Journal of The Electrochemical Society* 169 (2022) 090528. URL: <https://dx.doi.org/10.1149/1945-7111/ac91fb>, publisher: IOP Publishing.
 - [35] W. Ai, Y. Liu, JuBat: A Julia-based framework for battery modelling using finite element method, *SoftwareX* 27 (2024) 101760. URL: <https://linkinghub.elsevier.com/retrieve/pii/S2352711024001316>. doi:10.1016/j.softx.2024.101760.
 - [36] COMSOL Multiphysics® v. 6.3, Battery Design Module User’s Guide, COMSOL AB, Stockholm, Sweden, 2024.
 - [37] X. Yin, D. Zhang, batP2dFoam: An Efficient Segregated Solver for the Pseudo-2-Dimensional (P2D) Model of Li-Ion Batteries, *Journal of The Electrochemical Society* 170 (2023) 030521. URL: <https://dx.doi.org/10.1149/1945-7111/acbfe4>. doi:10.1149/1945-7111/acbfe4, publisher: IOP Publishing.
 - [38] W. Ai, Y. Liu, Improving the convergence rate of Newman’s battery model using 2nd order finite element method, *Journal of Energy Storage* 67 (2023) 107512. URL: <https://linkinghub.elsevier.com/retrieve/pii/S2352152X2300909X>. doi:10.1016/j.est.2023.107512.
 - [39] J. Kim, A. Mallarapu, S. Santhanagopalan, J. Newman, A robust numerical treatment of solid-phase diffusion in pseudo two-dimensional lithium-ion battery models, *Journal of Power Sources* 556

- (2023) 232413. URL: <https://linkinghub.elsevier.com/retrieve/pii/S0378775322013908>. doi:10.1016/j.jpowsour.2022.232413.
- [40] V. Thomée, Galerkin Finite Element Methods for Parabolic Problems, Springer, Berlin Heidelberg, 2007.
 - [41] R. Han, C. Macdonald, B. Wetton, A fast solver for the pseudo-two-dimensional model of lithium-ion batteries, 2021. URL: <http://arxiv.org/abs/2111.09251>, arXiv:2111.09251 [physics].
 - [42] A. Latz, J. Zausch, Multiscale modeling of lithium ion batteries: Thermal aspects, Beilstein Journal of Nanotechnology 6 (2015) 987–1007. URL: <https://www.beilstein-journals.org/bjnano/articles/6/102>. doi:10.3762/bjnano.6.102.
 - [43] J. M. O. a. W. C. Rheinboldt, Iterative Solution of Nonlinear Equations in Several Variables (Classics in Applied Mathematics), SIAM, 1987. URL: <http://gen.lib.rus.ec/book/index.php?md5=cf8fe5541f9d65562f5b058898c63ce5>.
 - [44] P. R. Brune, M. G. Knepley, B. F. Smith, X. Tu, Composing Scalable Nonlinear Algebraic Solvers, SIAM Review 57 (2015) 535–565. URL: <http://pubs.siam.org/doi/10.1137/130936725>. doi:10.1137/130936725.
 - [45] A. Latz, J. Zausch, Thermodynamic derivation of a Butler–Volmer model for intercalation in Li-ion batteries, Electrochimica Acta 110 (2013) 358–362. URL: <https://www.sciencedirect.com/science/article/pii/S0013468613011493>. doi:10.1016/j.electacta.2013.06.043.
 - [46] J. Wu, V. Srinivasan, J. Xu, C. Y. Wang, Newton-Krylov-Multigrid algorithms for battery simulation, Journal of The Electrochemical Society 149 (2002) A1342. URL: <https://iopscience.iop.org/article/10.1149/1.1505635>. doi:10.1149/1.1505635.
 - [47] P. G. Ciarlet, The Finite Element Method for Elliptic Problems, Society for Industrial and Applied Mathematics, Philadelphia, 2002.

- [48] J. Xu, Estimate of the convergence rate of finite element solutions to elliptic equations of second order with discontinuous coefficients, 2013.
URL: <https://arxiv.org/abs/1311.4178>. arXiv:1311.4178.
- [49] B. S. Kirk, J. W. Peterson, R. H. Stogner, G. F. Carey, **libMesh**: A C++ Library for Parallel Adaptive Mesh Refinement/Coarsening Simulations, *Engineering with Computers* 22 (2006) 237–254.
- [50] S. Balay, S. Abhyankar, M. F. Adams, J. Brown, P. Brune, K. Buschelman, L. Dalcin, A. Dener, V. Eijkhout, W. D. Gropp, D. Karpeyev, D. Kaushik, M. G. Knepley, D. A. May, L. C. McInnes, R. T. Mills, T. Munson, K. Rupp, P. Sanan, B. F. Smith, S. Zampini, H. Zhang, H. Zhang, PETSc Users Manual, Technical Report ANL-95/11 - Revision 3.15, Argonne National Laboratory, 2021. URL: <https://www.mcs.anl.gov/petsc>.
- [51] X. S. Li, J. W. Demmel, SuperLU_DIST: A scalable distributed-memory sparse direct solver for unsymmetric linear systems, *ACM Trans. Math. Softw.* 29 (2003) 110–140. URL: <https://doi.org/10.1145/779359.779361>. doi:10.1145/779359.779361.